Numerical analysis of the Factorization Method for Electrical Impedance Tomography in inhomogeneous medium

Houssem Haddar, Giovanni Migliorati

INSTITUT NATIONAL DE RECHERCHE EN INFORMATIQUE ET EN AUTOMATIQUE

Numerical analysis of the Factorization Method for Electrical Impedance Tomography in inhomogeneous medium

Houssem Haddar — Giovanni Migliorati

N° 7801

October 2011

Thème NUM

ISSN 0249-6399 ISRN INRIA/RR--7801--FR+ENG

INSTITUT NATIONAL
DE RECHERCHE
EN INFORMATIQUE
ET EN AUTOMATIQUE

INRIA

centre de recherche
SACLAY - ÎLE-DE-FRANCE

Numerical analysis of the Factorization Method for Electrical Impedance Tomography in inhomogeneous medium

Houssem Haddar* , Giovanni Migliorati†

Thème NUM — Systèmes numériques
Équipes-Projets DeFI

Rapport de recherche n° 7801 — October 2011 — 33 pages

Abstract: The retrieval of information on the coefficient in Electrical Impedance Tomography is a severely ill-posed problem, and often leads to inaccurate solutions. It is well-known that numerical methods provide only low-resolution reconstructions. The aim of this work is to analyze the Factorization Method in the case of inhomogeneous background. We propose a numerical scheme to solve the dipole-like Neumann boundary-value problem, when the background coefficient is inhomogeneous. Several numerical tests show that the method is able to detect the presence and location of the inclusions, in many cases where the diffusion coefficient depends nonlinearly on the spatial coordinates. In addition, we test the numerical scheme after adding artificial noise.

Key-words: Inverse Problems, Factorization Method, Electrical Impedance Tomography

* INRIA Saclay Île de France and École Polytechnique (CMAP)
† Dipartimento di Matematica "Francesco Brioschi", Politecnico di Milano and École Polytechnique (CMAP)

Centre de recherche INRIA Saclay – Île-de-France
Parc Orsay Université
4, rue Jacques Monod, 91893 ORSAY Cedex
Téléphone : +33 1 72 92 59 00

Rapport de Recherche
Inria

Résumé : Nous nous intéressons dans ce travail à l'application de la méthode de Factorization à l'imagerie par impédance électrique dans des milieux hétérogènes. Nous proposons un schéma numérique qui se base sur une évaluation précise de la fonction de Green du milieu. Plusieurs tests numériques sont effectués demontrant de bonnes performances de la méthode, très comparables au cas de milieux homogènes.

Mots-clés : Problèmes inverses, la méthode de factorisation, tomographie d'impédance électrique

1 Introduction

The problem of *Electrical Impedance Tomography* (EIT) arises in many applied contexts. It leads to well established operative procedures, *e.g.* in geophysics, nondestructive testing or imaging applications, while in other fields its usage is still experimental *e.g.* medicine, [4] [13] [18]. The rigorous framework of the EIT problem was set up for the first time by Calderón in his seminal paper [8]. Briefly, it concerns the determination of the coefficient of a given (elliptic) PDE model from the (complete or incomplete) knowledge of suitable maps, *e.g.* the *Dirichlet-to-Neumann map* (DtNm). In the isotropic case, the uniqueness of the solution to the two-dimensional conductivity inverse problem has been showed in the general L^∞ case in [3]. In three dimensions the uniqueness is proven if additional smoothness on the coefficient is assumed [5]. Concerning the stability, at the moment there exist only logarithmic-type estimates in two dimensions (and higher) [1]. The anisotropic case is much less complete. In general, even the complete knowledge of the DtNm does not allow to uniquely recover the coefficient, but some partial answers are present in the literature [16].

Many mathematical models for EIT were proposed, trying to take into account as many physical phenomena as possible. In this work we address the Factorization Method (see [14]) applied to the *Continuous Model* (CM) in the context of EIT featuring an inhomogeneous isotropic background. The aim is to recover the support of unknown inclusions from the knowledge of indirect boundary measurements. We propose a numerical scheme to solve the dipole-like Neumann boundary-value problem, when the background coefficient is inhomogeneous. We treat different types of nonlinearities in the coefficient, and show through several numerical tests that the method is able to detect the presence and location of the inclusions. Moreover, we investigate the robustness of the method applying a random perturbation to the measurement operator. We exhibit the better accuracy of the Tikhonov regularization (TR) with the Morozov principle, compared to the simple truncated Picard criterion (PC), which is commonly used in the literature.

1.1 Mathematical formulation

Consider a bounded domain $B \subset \mathbb{R}^2$ and its subset $D \subset B$, see Figure 1. We assume that B is a C^2–domain, but it could be Lipschitz as well. Moreover, we assume that D is a union of possibly disjoint Lipschitz domains, each one with positive measure, and that $B \setminus \overline{D}$ is connected. The domain B represents the background medium, modeled by the diffusion coefficient σ_B. The domain D represents an inclusion, displaced somewhere inside B, but not too close to the boundary ∂B. The inclusion is characterized by unknown shape and unknown value of its diffusion coefficient σ_D.

In the last decades a lot of efforts have been dedicated to the research of the minimal regularity assumptions for the coefficients σ_B, σ_D, in order for the EIT problem to be well-posed. The theory behind EIT does not present any substantial differences between the cases of homogeneous and inhomogeneous background. However, the inhomogeneous background case is numerically much less investigated. We will consider only homogeneous inclusions, since our main target is the inhomogeneity in the background. The next assumption recaps the case we will focus on, including some technical requirements.

Assumption 1. *Assume σ_B is α-Holderian in B with $\alpha > 1$. Moreover, denoting by*

$$\sigma_B^m = \min_{x \in B} \sigma_B(x) \quad \text{and} \quad \sigma_B^M = \max_{x \in B} \sigma_B(x),$$

then σ_B and σ_D satisfy

$$0 < \sigma_D < \sigma_B^m < \sigma_B^M < \infty, \quad \text{or} \quad 0 < \sigma_B^m < \sigma_B^M < \sigma_D < \infty.$$

Remark 1. *In our numerical scheme the requirement that σ_B is α-Holderian in B can be easily extended to $\sigma_B \in L^\infty(B)$, choosing the sampling points such that they do not fall exactly where σ_B jumps.*

Now consider the coefficient $\sigma(\boldsymbol{x}) \in L^\infty(B)$ defined as

$$\sigma(\mathbf{x}) = \begin{cases} \sigma_B(\mathbf{x}), & \text{in } B \setminus D, \\ \sigma_D(\mathbf{x}), & \text{in } D, \end{cases} \tag{1.1}$$

and define the functional spaces

$$\mathring{L}^2(\partial B) = \Big\{ g \in L^2(\partial B), \int_{\partial B} g = 0 \Big\}, \quad \mathring{H}^1(B) = \Big\{ g \in H^1(B), \int_{\partial B} g = 0 \Big\},$$

$$\mathring{H}^{\frac{1}{2}}(\partial B) = \Big\{ g \in H^{\frac{1}{2}}(\partial B), \int_{\partial B} g = 0 \Big\}, \quad \mathring{H}^{-\frac{1}{2}}(\partial B) = \Big\{ g \in H^{-\frac{1}{2}}(\partial B),\ {}_{H^{-1/2}}\langle g, 1 \rangle_{H^{1/2}} = 0 \Big\}.$$

Given $g \in \mathring{H}^{-\frac{1}{2}}(\partial B)$, consider the elliptic Neumann boundary-value problem

$$\begin{cases} \nabla \cdot (\sigma(\mathbf{x}) \nabla u) = 0, & \text{in } B, \\ \boldsymbol{\nu} \cdot \nabla u = g, & \text{on } \partial B. \end{cases} \tag{1.2}$$

The existence of a family of solutions is ensured from Theorem 10 when the function g satisfies the usual compatibility condition and the coefficient σ defined in (1.1) satisfies Assumption 1. To uniquely select a solution we pick the one with null mean on the boundary ∂B.

Proposition 1. *Under Assumption 1, it holds $\sigma \in L^\infty(B)$, and for every $g \in \mathring{H}^{-\frac{1}{2}}(\partial B)$ there exists a unique solution $u \in \mathring{H}^1(B)$ to problem* (1.2).

In the EIT problem we prescribe a current pattern g and we measure the generated potential $f = u\big|_{\partial B}$ on the boundary ∂B. The final aim is to retrieve some information about D, *e.g.* its presence and location inside B. The operator Λ that maps currents g into potentials f is the

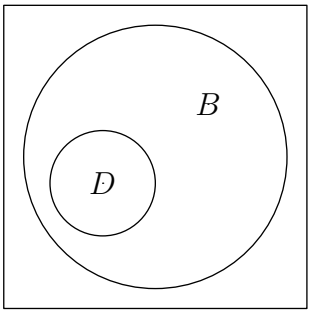

Fig. 1: An inclusion D which lies in a medium B.

Neumann-to-Dirichlet map (NtDm) associated with problem (1.2) with the coefficient (1.1). It is a continuos operator from $\mathring{H}^{-\frac{1}{2}}(\partial B)$ to $\mathring{H}^{\frac{1}{2}}(\partial B)$. Its restriction $\Lambda : \mathring{L}^2(\partial B) \to \mathring{L}^2(\partial B)$ is compact also. Denote by Λ_0 the NtDm associated with the problem (1.2) with the coefficient

$$\sigma(\mathbf{x}) = \sigma_B(\mathbf{x}), \text{ in } B, \tag{1.3}$$

and by u_0 the solution to the same problem. In this way u_0 represents the potential generated by the incoming current g in the domain B, when the inclusion D is not present. Let f_0 be the corresponding measured potential $f_0 = u_0\big|_{\partial B} = \Lambda_0 g$. Moreover, we define the operator $\widetilde{\Lambda}$ that will play a central role in the sequel:

$$\widetilde{\Lambda} := \Lambda - \Lambda_0 : \mathring{L}^2(\partial B) \to \mathring{L}^2(\partial B). \tag{1.4}$$

Remark 2. *The case $\sigma_D = 0$ and $\sigma_D = +\infty$ are allowed as well, and are known as perfectly insulating and perfectly conducting inclusions, but they require a slightly different treatment.*

We will need also the Green function $N(\cdot,\boldsymbol{\xi}) \in \mathring{L}^2(B)$, which is a solution to the following Neumann boundary-value problem with a singular source δ_ξ centered in the point $\boldsymbol{\xi} \in B$:

$$\begin{cases} \nabla_1 \cdot (\sigma_B(\mathbf{x})\nabla_1 N(\mathbf{x},\boldsymbol{\xi})) = -\delta_\xi(\mathbf{x}), & \mathbf{x} \in B, \\ \boldsymbol{\nu} \cdot \nabla_1 N(\mathbf{x},\boldsymbol{\xi}) = -\dfrac{1}{|B|}, & \mathbf{x} \text{ on } \partial B. \end{cases} \tag{1.5}$$

Notice that (1.5) does not embed any information about the inclusion D. Denote by $\mathbf{p}$ a two-dimensional versor (*i.e.* $|\mathbf{p}| = 1$). In the sequel we will often need the scalar product

$$\psi(\mathbf{x},\boldsymbol{\xi},\mathbf{p}) := \mathbf{p} \cdot \nabla_2 N(\mathbf{x},\boldsymbol{\xi}), \quad \mathbf{x} \in B, \tag{1.6}$$

as well as its restriction on ∂B

$$l^p_\xi = \psi(\mathbf{x},\boldsymbol{\xi},\mathbf{p})\Big|_{\mathbf{x} \text{ on } \partial B}. \tag{1.7}$$

Moreover, denoting by $\{\mathbf{e}_1, \mathbf{e}_2\}$ an orthonormal basis of $\mathbb{R}^2$, we denote

$$l^k_\xi = l^{e_k}_\xi, \quad k = 1, 2.$$

When the domain B is a circle with radius R, there is an explicit formula for the solution $N(\mathbf{x},\boldsymbol{\xi})$ to the Neumann problem (1.5) with $\sigma_B \equiv 1$ (see *e.g.* [2]):

$$N(\mathbf{x},\boldsymbol{\xi}) = -\frac{1}{2\pi}\left(\log|\mathbf{x}-\boldsymbol{\xi}| + \log\left|\frac{R}{|\mathbf{x}|}\mathbf{x} - \frac{|\mathbf{x}|}{R}\boldsymbol{\xi}\right|\right) + \frac{\log R}{\pi}. \tag{1.8}$$

One can check that $N(\mathbf{x},\boldsymbol{\xi}) \in \mathring{H}^1(B \setminus \mathcal{O}_\xi)$, with $\mathcal{O}_\xi$ being an arbitrarily small neighborhood of $\boldsymbol{\xi}$. See *e.g.* Theorem 2. Notice that only the first logarithm can yield a singularity, since the second one is singular only when $\boldsymbol{\xi}$ falls on the boundary, *i.e.* if $|\mathbf{x}| \le R$ and $|\boldsymbol{\xi}| < R$ then

$$\left|\frac{R}{|\mathbf{x}|}\mathbf{x} - \frac{|\mathbf{x}|}{R}\boldsymbol{\xi}\right| \ge \left|\left|\frac{R}{|\mathbf{x}|}\mathbf{x}\right| - \left|\frac{|\mathbf{x}|}{R}\boldsymbol{\xi}\right|\right| = \left|R - \frac{|\mathbf{x}|\,|\boldsymbol{\xi}|}{R}\right| > 0.$$

Moreover, one can check that $N(\cdot,\cdot)$ is a symmetric function.

In the case where (1.8) holds, we have an explicit formula for the evaluation of ψ defined in (1.6) on the boundary of the unitary circle [6]:

$$\psi(\mathbf{x},\boldsymbol{\xi},\mathbf{p})\Big|_{\partial B} = \frac{1}{\pi}\frac{\mathbf{p}\cdot(\boldsymbol{\xi}-\mathbf{x})}{|\boldsymbol{\xi}-\mathbf{x}|^2}, \qquad \text{for } |\mathbf{x}| = 1.$$

2 Sampling Methods for EIT

The most famous sampling methods are the *Linear Sampling* (LS) and the *Factorization Method* (FM). The former was introduced in its modern form for scattering problems by *D.Colton et. al* in the middle '90, while the latter was introduced some years later by *A.Kirsch*. These methods can be classified as shape identification methods, since they allow to recover the shape of unknown contrast objects from indirect measurements.

Both the LS and FM have been extended also to the EIT framework, and are widely studied in the literature nowadays. We will focus on the FM. The application of the FM applied to the Complete Electrode Model has been investigated in [15].

2.1 The case of small inclusions

Denote by $C_\tau(\boldsymbol{\xi}) \subset \mathbb{R}^2$ a circle centered in $\boldsymbol{\xi} \in \mathbb{R}^2$ with radius equal to τ.

Definition 1. *Let $d_0 > 0$ be constant. Given M points $\boldsymbol{\xi}_1, \ldots, \boldsymbol{\xi}_M$ in B such that dist$(\boldsymbol{\xi}_i, \boldsymbol{\xi}_j) \geq d_0$, $\forall i \neq j$, and dist$(\boldsymbol{\xi}_i, \partial B) \geq d_0$, $\forall j$, define for each j the inclusion $C_\tau(\boldsymbol{\xi}_j)$ with its coefficient σ_{D_j}. Define D as $D = \cup_{j=1}^M C_\tau(\boldsymbol{\xi}_j)$. The background coefficient σ_B can be inhomogeneous. If the parameter τ is small then we refer to this situation as* small inclusion case. *Under this assumption it is reasonable to assume the coefficient σ_{D_j} inside each inclusion to be homogeneous, but always satisfying Assumption 1.*

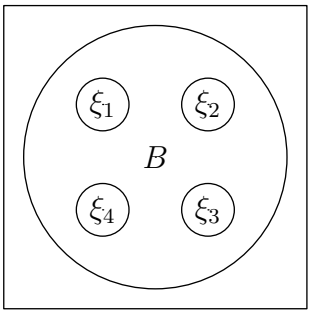

Fig. 2: Several inclusions which lie in a medium B. This figure displays $M = 4$ circular inclusions which are centered in the points $\boldsymbol{\xi}_1, \boldsymbol{\xi}_2, \boldsymbol{\xi}_3, \boldsymbol{\xi}_4$ and have a radius equal to τ.

The next result was first given in [9] under the strong assumption $\sigma(\mathbf{x}) \in C^\infty(B)$, and then extended in [7]. It relates the solutions $N(\mathbf{x}, \cdot)$ to problem (1.5) with the difference bewteen the solution u of problem (1.2) with the coefficient (1.1) and the solution u_0 of the same problem (1.2) but with the coefficient (1.3).

Theorem 1. *In the* small inclusion case, *when $\tau \downarrow 0$ the solution of problem* (1.1) *can be expanded as*

$$u(\mathbf{x}) = u_0(\mathbf{x}) + \tau^2 \sum_{j=1}^{M} \lambda_j \nabla_1 N(\boldsymbol{\xi}_j, \mathbf{x}) \cdot M_j \, \nabla u_0(\boldsymbol{\xi}_j) + \mathcal{O}(\tau^{5/2}), \quad \forall \mathbf{x} \in \partial B, \tag{2.1}$$

with

$$\lambda_j = \sigma_B(\boldsymbol{\xi}_j) \frac{\sigma_B(\boldsymbol{\xi}_j) - \sigma_{D_j}}{\sigma_{D_j}}.$$

Here M_j is the polarization tensor corresponding to the jth inhomogeneity. It is a symmetric positive definite 2×2 matrix.

Corollary 1 (Corollary of Theorem 1)**.** *Under the assumptions of Theorem 1, when $\sigma_B \equiv 1$ the expansion* (2.1) *for $\tau \downarrow 0$ holds with*

$$\lambda_j = \frac{(1 - \sigma_{D_j})}{\sigma_{D_j}}.$$

Moreover, if the inclusion D_j has a circular shape then

$$M_j = |D_j| \begin{pmatrix} \dfrac{2\sigma_{D_j}}{1 + \sigma_{D_j}} & 0 \\ 0 & \dfrac{2\sigma_{D_j}}{1 + \sigma_{D_j}} \end{pmatrix}.$$

Remark 3. *Denote by $E : \mathring{L}^2(\partial B) \to \mathring{L}^2(\partial B)$ the operator*

$$Eg = \sum_{j=1}^{M} \lambda_j \nabla_1 N(\boldsymbol{\xi}_j, \cdot) \cdot M_j \, \nabla u_0(\boldsymbol{\xi}_j),$$

where $u_0 \in \mathring{H}^1(B)$ *is the solution to problem* (1.2) *with the coefficient* (1.3). *Then we can express* $\widetilde{\Lambda}$ *introduced in* (1.4) *as*

$$\widetilde{\Lambda} = \tau^2 E + \mathcal{O}(\tau^{5/2}). \tag{2.2}$$

Theorem 2. *The problem*

$$\begin{cases} \Delta N(\mathbf{x}, \boldsymbol{\xi}) = -\delta_\xi(\mathbf{x}), & \mathbf{x} \in B, \\ \dfrac{\partial N(\mathbf{x}, \boldsymbol{\xi})}{\partial \boldsymbol{\nu}} = -\dfrac{1}{|B|}, & \mathbf{x} \text{ on } \partial B, \end{cases} \tag{2.3}$$

has a unique solution in $\mathring{H}^1_{loc}(B \setminus \{\boldsymbol{\xi}\}) \cap L^2(B)$.

Proof of Theorem 2. Given $\boldsymbol{\xi} \in B$, the function

$$\phi(\cdot, \boldsymbol{\xi}) = -\frac{1}{2\pi} \log|\cdot - \boldsymbol{\xi}|$$

is a solution of the problem

$$\Delta\phi(\cdot, \boldsymbol{\xi}) = -\delta_\xi(\cdot), \text{ in } \mathbb{R}^2.$$

We observe that $\forall \varepsilon > 0$

$$\int_{\partial B} \frac{\partial \phi(\cdot, \boldsymbol{\xi})}{\partial \boldsymbol{\nu}}\, ds = \int_{|\mathbf{x}-\boldsymbol{\xi}|=\varepsilon} \frac{\partial \phi(\varepsilon e^\theta, \boldsymbol{\xi})}{\partial \boldsymbol{\nu}}\, \varepsilon\, d\theta = -\frac{\varepsilon}{2\pi} \int_0^{2\pi} \frac{1}{\varepsilon} = -1. \tag{2.4}$$

Now define the function $\varphi_N(\cdot, \boldsymbol{\xi}) = N(\cdot, \boldsymbol{\xi}) - \phi(\cdot, \boldsymbol{\xi})$, and consider the problem

$$\begin{cases} \Delta\varphi_N(\cdot, \boldsymbol{\xi}) = 0, & \text{in } B, \\ \dfrac{\partial \varphi_N(\cdot, \boldsymbol{\xi})}{\partial \boldsymbol{\nu}} = -\dfrac{\partial \phi(\cdot, \boldsymbol{\xi})}{\partial \boldsymbol{\nu}} - \dfrac{1}{|\partial B|}, & \text{on } \partial B, \end{cases}$$

which has a unique solution $\varphi_N \in \mathring{H}^1(B)$ since, due to (2.4), $\dfrac{\partial \phi(\cdot, \boldsymbol{\xi})}{\partial \boldsymbol{\nu}} + \dfrac{1}{|\partial B|} \in \mathring{H}^{-\frac{1}{2}}(\partial B)$. In addition $\varphi_N \in H^2(\partial B)$ because of the regularity on the boundary and $\dfrac{\partial \phi(\cdot, \boldsymbol{\xi})}{\partial \boldsymbol{\nu}} + \dfrac{1}{|\partial B|} \in \mathring{H}^{\frac{1}{2}}(\partial B)$. So we have built a function

$$N(\cdot, \boldsymbol{\xi}) = \phi(\cdot, \boldsymbol{\xi}) + \varphi_N(\cdot, \boldsymbol{\xi})$$

which is a solution to problem (2.3). Moreover, we notice that $N(\cdot, \boldsymbol{\xi}) \notin \mathring{H}^1(B)$ due to the singularity in $\boldsymbol{\xi}$ of $\phi(\cdot, \boldsymbol{\xi})$. □

In the case of small inclusions it is possible to characterize directly the support of the inclusions D through the range of the operator E. See [7] for the proof of the following theorem.

Theorem 3. *Range*$(E) = span\Big\{ l^k_{\xi_j}, \quad j = 1, \dots, M, \quad k = 1, 2 \Big\}$.

Notice that Range(E) has finite dimension, since it is the span of $2M$ functions.

Theorem 4 (Unique continuation)**.** *Let* $O \subset \mathbb{R}^2$ *be an open connected set. If the following conditions hold*

- $u \in C^2(O)$,
- $|\Delta u(\mathbf{x})| \le C(|\nabla u(\mathbf{x})| + u(\mathbf{x})), \quad \forall \mathbf{x} \in O$,
- $u = 0$ *in a neighborhood of some* $\mathbf{x}_0 \in O$,

then $u \equiv 0$ *in* O.

Theorem 5. *Let* $\mathbf{p} \in \mathbb{R}^2$, $|\mathbf{p}| = 1$. *Then* $l^p_\xi \in$ *Range*$(E) \iff \boldsymbol{\xi} \in \{\boldsymbol{\xi}_j, j = 1, \dots, M\}$.

Proof of Theorem 5. Suppose that $\boldsymbol{\xi} \notin \{\boldsymbol{\xi}_j, j = 1, \ldots, M\}$. If $l^p_\xi \in \text{Range}(E)$, then there exist a suitable g and a suitable $\widetilde{u}$ such that

$$l^p_\xi = Eg = \widetilde{u}\Big|_{\partial B}.$$

On the other hand, the values $\mathbf{p}$ and $\boldsymbol{\xi}$ in l^p_ξ uniquely determine the solution of problem (2.3), and thus the function ψ through (1.7). So $\psi\big|_{\partial B} = \widetilde{u}\big|_{\partial B}$. From (2.1) we see that $\widetilde{u}$ is a linear combination with coefficients $\alpha_1, \ldots, \alpha_M$ of the functions $\nabla_1 N(\boldsymbol{\xi}_j, \mathbf{x})$,

$$\widetilde{u}(\mathbf{x}) = \sum_{j=0}^{M} \alpha_j \nabla_1 N(\boldsymbol{\xi}_j, \mathbf{x}), \tag{2.5}$$

and then we have also

$$\frac{\partial \psi}{\partial \boldsymbol{\nu}}\bigg|_{\partial B} = \frac{\partial \widetilde{u}}{\partial \boldsymbol{\nu}}\bigg|_{\partial B}.$$

Therefore the function $w = \widetilde{u} - \psi$ satisfies

$$\begin{cases} w = 0, & \text{on } \partial B, \\ \dfrac{\partial w}{\partial \nu} = 0, & \text{on } \partial B, \\ \Delta w = 0, & \text{in } B \setminus \{\boldsymbol{\xi}, \boldsymbol{\xi}_1, \ldots, \boldsymbol{\xi}_M\}, \end{cases}$$

and $w \in H^2_{loc}(B \setminus \{\boldsymbol{\xi}, \boldsymbol{\xi}_1, \ldots, \boldsymbol{\xi}_M\})$. Now take $\widetilde{w}$ such that

$$\begin{cases} \widetilde{w} = 0, & \text{in } \mathbb{R}^2 \setminus B, \\ \widetilde{w} = w, & \text{in } B \setminus \{\boldsymbol{\xi}, \boldsymbol{\xi}_1, \ldots, \boldsymbol{\xi}_M\}. \end{cases}$$

Then, denoting with $[\cdot]$ the jump, $\widetilde{w}$ also satisfies

$$[\widetilde{w}] = 0, \text{ on } \partial B, \qquad \left[\frac{\partial \widetilde{w}}{\partial \nu}\right] = 0, \text{ on } \partial B,$$

$$\Delta \widetilde{w} = \begin{cases} 0, & \text{in } B \setminus \{\boldsymbol{\xi}, \boldsymbol{\xi}_1, \ldots, \boldsymbol{\xi}_M\}, \\ 0, & \text{in } \mathbb{R}^2 \setminus B. \end{cases}$$

So in the end,

$$\begin{aligned} \Delta \widetilde{w} = 0, \text{ in } \mathbb{R}^2 \setminus \{\boldsymbol{\xi}, \boldsymbol{\xi}_1, \ldots, \boldsymbol{\xi}_M\}, \\ \widetilde{w} = 0, \text{ in } \mathbb{R}^2 \setminus B. \end{aligned}$$

Thanks to Theoerm 4, $\psi = \widetilde{u}$ in $B \setminus \{\boldsymbol{\xi}, \boldsymbol{\xi}_1, \ldots, \boldsymbol{\xi}_M\}$. Being O_ξ a neighborhood of $\boldsymbol{\xi}$ that does not intersect $\{\boldsymbol{\xi}_1, \ldots, \boldsymbol{\xi}_M\}$, we have a contradiction since $\widetilde{u} \in H^1(O_\xi)$ (from (2.5)), but $\psi \notin H^1(O_\xi)$. The opposite implication is straightforward, from the characterization in Theorem 3. □

See [7] for a detailed description of how to relate the range of the operators E and $\widetilde{\Lambda}$, which are related each other by (2.2). In the next section we derive the characterization through the range of $\widetilde{\Lambda}^{1/2}$ of the support of inclusions with arbitrary shape.

2.2 The Factorization Method for EIT

In this section we outline the basis of the FM applied to EIT. The main result is the factorization of the operator $\widetilde{\Lambda}$ given in Theorem 6, (see [17, Chap.12,Thm.4] for a proof). In [14] a more general

three-term factorization is derived for $\widetilde{\Lambda} : \mathring{H}^{-1/2}(\partial B) \to \mathring{H}^{1/2}(\partial B)$. Also another simpler two-term factorization can be chosen, see *e.g.* [17]. Although many factorizations are possible, each one of them provides a necessary and sufficient criterion to determine the inclusions. Lemma 1 and Theorem 9 show how this criterion becomes operative.

Let us introduce the operator $G : \mathring{H}^{-1/2}(\partial D) \to \mathring{L}^2(\partial B)$. It acts as a NtDm of a suitable virtual problem,

$$\begin{cases} \nabla \cdot (\sigma_B(\mathbf{x}) \nabla w) = 0, & \text{in } B \setminus \overline{D}, \\ \dfrac{\partial w}{\partial \nu} = 0, & \text{on } \partial B, \\ -\dfrac{\partial w}{\partial \nu} = \varphi, & \text{on } \partial D, \end{cases} \tag{2.6}$$

where $\varphi \in \mathring{H}^{-1/2}(\partial D)$ is the input, and $w\big|_{\partial B} \in \mathring{L}^2(\partial B)$ is the output. Moreover, define the space $W = \{w \in \mathring{H}^1(B \setminus \overline{D}) : w \text{ solves } (2.6)\}$, and denote by $G^* : \mathring{L}^2(\partial B) \to \mathring{H}^{1/2}(\partial D)$ the adjoint of G. To define the operator T we introduce the problems

$$\begin{cases} \nabla \cdot (\sigma(\mathbf{x}) \nabla \varpi) = 0, & \text{in } B \setminus \partial D, \\ \dfrac{\partial \varpi}{\partial \nu} = 0, & \text{on } \partial B, \\ [\varpi]_{\partial D} = \varphi, & \text{on } \partial D, \\ [\boldsymbol{\nu} \cdot \sigma(\mathbf{x}) \nabla \varpi]_{\partial D} = 0, & \text{on } \partial D, \\ \int_{\partial B} \varpi \, ds = 0, \end{cases} \qquad \begin{cases} \nabla \cdot (\sigma_B(\mathbf{x}) \nabla \varpi_0) = 0, & \text{in } B \setminus \partial D, \\ \dfrac{\partial \varpi_0}{\partial \nu} = 0, & \text{on } \partial B, \\ [\varpi_0]_{\partial D} = \varphi, & \text{on } \partial D, \\ [\boldsymbol{\nu} \cdot \sigma_B(\mathbf{x}) \nabla \varpi_0]_{\partial D} = 0, & \text{on } \partial D, \\ \int_{\partial B} \varpi_0 \, ds = 0. \end{cases}$$

The operator T is defined as

$$T : \mathring{H}^{1/2}(\partial D) \to \mathring{H}^{-1/2}(\partial D) : \varphi \mapsto \left. \frac{\partial (\varpi^+ - \varpi_0^+)}{\partial \boldsymbol{\nu}} \right|_{\partial D},$$

where ϖ^+ and ϖ_0^+ are the restrictions of ϖ and ϖ_0 on $B \setminus \overline{D}$.

Theorem 6. *The operator $\widetilde{\Lambda} : \mathring{L}^2(\partial B) \to \mathring{L}^2(\partial B)$ introduced in* (1.4) *can be factorized as*

$$\widetilde{\Lambda} = GTG^*.$$

Theorem 7. *A point $\boldsymbol{\xi} \in B$ belongs to D if and only if l^p_ξ coincides with the trace of any potential $w \in W$.*

Proof. Let $\boldsymbol{\xi} \in D$. From the definition (1.7) we know that l^p_ξ is the trace of $\psi(\cdot, \boldsymbol{\xi}, \mathbf{p}) \in \mathring{H}^1(B \setminus \overline{D})$. For every $\boldsymbol{\xi}$ the function $N(\cdot, \boldsymbol{\xi})$ has the same Neumann data on the boundary. Thus its normal derivative w.r.t. $\boldsymbol{\xi}$ is null on ∂B. Moreover, on each connected component of D, the *Green's formula* gives

$$\int_{\partial D_j} \nabla_2 \psi(\mathbf{x}, \boldsymbol{\xi}, \mathbf{p}) \cdot \boldsymbol{\nu} \, ds = 0, \tag{2.7}$$

for every component $D_j \subset D$ such that $\boldsymbol{\xi} \notin D_j$. But also the flux of $\psi(\cdot, \boldsymbol{\xi}, \mathbf{p})$ across $\partial(B \setminus \overline{D})$ vanishes, so (2.7) holds also for the component D_j of D such that $\boldsymbol{\xi} \in D_j$. Therefore $\psi(\cdot, \boldsymbol{\xi}, \mathbf{p}) \in W$.

In the case $\boldsymbol{\xi} \notin \overline{D}$, if $\exists w \in W$ such that l^p_ξ is the trace of w then we obtain a contradiction. In fact, w and $\psi(\cdot, \boldsymbol{\xi}, \mathbf{p})$ (related to l^p_ξ by (1.7)) satisfy the same Neumann problem in $B \setminus (\overline{D} \cup \{\boldsymbol{\xi}\})$ with the same boundary conditions. The uniqueness of the solution implies that w and $\psi(\cdot, \boldsymbol{\xi}, \mathbf{p})$ coincide in $B \setminus (\overline{D} \cup \{\boldsymbol{\xi}\})$. But now w extends harmonically into a neighborhood $\mathcal{O}(\boldsymbol{\xi})$ of $\boldsymbol{\xi}$, so that w is bounded in $\mathcal{O}(\boldsymbol{\xi})$ while $\psi(\cdot, \boldsymbol{\xi}, \mathbf{p})$ is not.

If $\boldsymbol{\xi} \in \partial D$ with the same argument w and $\psi(\cdot, \boldsymbol{\xi}, \mathbf{p})$ coincide in $B \setminus (\overline{D})$. But this is a contradiction because $w \in \mathring{H}^1(\mathcal{O}(\boldsymbol{\xi}) \cap (B \setminus (\overline{D}))$, but $\psi(\cdot, \boldsymbol{\xi}, \mathbf{p})$ has the singularity in $\boldsymbol{\xi}$. □

Lemma 1. *A point $\boldsymbol{\xi} \in B$ belongs to D if and only if $l^p_\xi \in Range(G)$.*

Proof. For any $\varphi \in \mathring{H}^{-1/2}(\partial D)$ the problem (2.6) has a unique solution $w \in W$. Vice-versa, every function $w \in W$ is a solution to problem (2.6), with a well-defined normal derivative $\varphi \in \mathring{H}^{-1/2}(\partial D)$. The thesis follows as a consequence of Theorem 7. □

Remark 4. *The space $\mathring{H}^{1/2}(\partial D)$ is a Banach reflexive space, with dual containing $\mathring{H}^{-1/2}(\partial D)$.*

Theorem 8. *The operator $T : \mathring{H}^{1/2}(\partial D) \to \mathring{H}^{-1/2}(\partial D)$ is self adjoint and coercive over $\mathring{H}^{1/2}(\partial D)$.*

Theorem 9. *Let $\widetilde{\Lambda} : \mathring{L}^2(\partial B) \to \mathring{L}^2(\partial B)$ and $G : \mathring{H}^{-1/2}(\partial D) \to \mathring{L}^2(\partial B)$ and $T : \mathring{H}^{1/2}(\partial D) \to \mathring{H}^{-1/2}(\partial D)$. In addition, let G be injective with dense range and let T be self adjoint and coercive on $Range(G^*)$. Then $Range(G) = Range(\widetilde{\Lambda}^{1/2})$ and*

$$y \in Range(G) \quad \Longleftrightarrow \quad \sum_{j=1}^{\infty} \frac{|(y, y_j)_Y|^2}{\lambda_j} < \infty, \tag{2.8}$$

where $\{\lambda_j, y_j \,:\, j \in J\}$ denotes a spectral system of the self adjoint and compact operator $\widetilde{\Lambda} = GTG^*$.

See [17, Chap.12] for the proof of Theorems 6, 8, 9.

2.3 Inhomogeneous background

In this section we show our approach to numerically solve the singular problem (1.5) when the coefficient σ_B is inhomogeneous. To overcome the singularity in the forcing term, we resort to the fundamental solution

$$\phi(\cdot, \boldsymbol{\xi}) = -\frac{1}{2\pi\sigma_B(\boldsymbol{\xi})} \log \Big| \cdot - \boldsymbol{\xi} \Big|, \quad \mathbf{x} \in \mathbb{R}^2,$$

of the problem

$$-\nabla \cdot \Big(\sigma_B(\boldsymbol{\xi}) \nabla \phi(\cdot, \boldsymbol{\xi}) \Big) = \delta_\xi, \quad \text{in } \mathbb{R}^2. \tag{2.9}$$

Since the singularity at $\boldsymbol{\xi}$ in problem (1.5) is of the same kind as in problem (2.9), we can restrict problem (1.5) in a small neighborhood $\mathcal{O}(\boldsymbol{\xi}) \subset \mathbb{R}^2$ of $\boldsymbol{\xi}$ where

$$\sigma_B(\mathbf{x}) \approx \sigma_B(\boldsymbol{\xi}), \qquad \forall\, \mathbf{x} \in \mathcal{O}(\boldsymbol{\xi}),$$

and approximate the solution $N(\mathbf{x}, \boldsymbol{\xi})$ of problem (1.5) near the singularity in $\boldsymbol{\xi}$ as

$$N(\mathbf{x}, \boldsymbol{\xi}) \approx \phi(\mathbf{x}, \boldsymbol{\xi}), \qquad \forall\, \mathbf{x} \in \mathcal{O}(\boldsymbol{\xi}).$$

Then we can write a nonsingular problem for the difference

$$\varphi_N(\cdot, \boldsymbol{\xi}) = N(\cdot, \boldsymbol{\xi}) - \phi(\cdot, \boldsymbol{\xi}), \tag{2.10}$$

plugging (2.10) in (1.5):

$$\begin{cases} -\nabla_x \cdot \Big(\sigma_B(\mathbf{x}) \nabla_1 \varphi_N(\mathbf{x}, \boldsymbol{\xi}) \Big) = -\nabla_x \cdot \left(\Big(\sigma_B(\boldsymbol{\xi}) - \sigma_B(\mathbf{x}) \Big) \nabla_1 \phi(\mathbf{x}, \boldsymbol{\xi}) \right), & \mathbf{x} \text{ in } B, \\ \sigma_B(\mathbf{x})\, \nabla_1 \varphi_N(\mathbf{x}, \boldsymbol{\xi}) \cdot \boldsymbol{\nu} = -\sigma_B(\mathbf{x})\, \nabla_1 \phi(\mathbf{x}, \boldsymbol{\xi}) \cdot \boldsymbol{\nu} - \dfrac{1}{|\partial B|}, & \mathbf{x} \text{ on } \partial B. \end{cases} \tag{2.11}$$

The forcing term in this problem still contains the term $\nabla_1 \phi(\cdot, \boldsymbol{\xi})$ which blows up approaching $\boldsymbol{\xi}$, but now it is multiplied by a vanishing coefficient. Moreover, the weak formulation of (2.11) reads

$$\text{find } \varphi_N \in \mathring{H}^1(B) \text{ such that } \int_B \sigma_B(\mathbf{x}) \nabla_1 \varphi_N(\mathbf{x}, \boldsymbol{\xi}) \cdot \nabla v \, d\mathbf{x} = \int_B \Big(\sigma_B(\boldsymbol{\xi}) - \sigma_B(\mathbf{x}) \Big) \nabla_1 \phi(\mathbf{x}, \boldsymbol{\xi}) \cdot \nabla v \, d\mathbf{x} + \\ + \int_{\partial B} \left(-\sigma_B(\boldsymbol{\xi}) \nabla_1 \phi(\mathbf{x}, \boldsymbol{\xi}) \cdot \boldsymbol{\nu} - \frac{1}{|\partial B|} \right) v \, ds, \quad \forall\, v \in H^1(B).$$

Lemma 2. *If $\sigma_B(\cdot)$ is α-Holderian in B with $\alpha > 0$,* i.e. $\exists\, 0 < K < \infty$ *such that*

$$|\sigma_B(\mathbf{x}_1) - \sigma_B(\mathbf{x}_2)| \leq K\,|\mathbf{x}_1 - \mathbf{x}_2|^\alpha, \quad \forall\, \mathbf{x}_1, \mathbf{x}_2 \in B, \tag{2.12}$$

then the linear functional

$$F(w) = \int_B \Big(\sigma_B(\boldsymbol{\xi}) - \sigma_B(\mathbf{x})\Big)\nabla_1\phi(\mathbf{x},\boldsymbol{\xi}) \cdot \nabla w \, d\mathbf{x},$$

is bounded on $H^1(B)$.

Proof of Lemma 2. The function $\zeta(\mathbf{x}) = \Big(\sigma_B(\boldsymbol{\xi}) - \sigma_B(\mathbf{x})\Big)\nabla_1\phi(\mathbf{x},\boldsymbol{\xi})$ belongs to $L^2(B)$ if $\alpha > 0$, thus

$$|F(w)| = \left| \int_B \zeta(\mathbf{x}) \cdot \nabla w \, d\mathbf{x} \right| \leq \Big\|\zeta\Big\|_{L^2(B,\mathbb{R}^2)} \Big\|\nabla w\Big\|_{L^2(B,\mathbb{R}^2)}, \quad \forall\, w \in H^1(B).$$

□

In the quantity ψ defined in (1.6), the dependence of $N(\cdot,\cdot)$ on the second argument is smooth. So we can exploit this regularity to derive a numerical scheme that given $\boldsymbol{\xi} \in B$ directly computes $\nabla_2 N(\cdot,\boldsymbol{\xi})$. To this aim we differentiate (2.10) with respect to the second argument, and obtain

$$\nabla_2\varphi_N(\cdot,\boldsymbol{\xi}) = \nabla_2 N(\cdot,\boldsymbol{\xi}) - \nabla_2\phi(\cdot,\boldsymbol{\xi}).$$

Since $\psi(\cdot,\boldsymbol{\xi},\mathbf{p})$ is a solution of problem (1.5) for any $\mathbf{p}$, then we can derive a numerical scheme to compute $\nabla_2 N(\cdot,\boldsymbol{\xi})$. The derivatives of ϕ w.r.t. $\boldsymbol{\xi}$ are

$$\frac{\partial\phi(\cdot,\boldsymbol{\xi})}{\partial\xi_k} = \frac{1}{2\pi\sigma_B(\boldsymbol{\xi})^2}\frac{\partial\sigma_B(\boldsymbol{\xi})}{\partial\xi_k}\log\Big(|\mathbf{x}-\boldsymbol{\xi}|\Big) + \frac{x_k - \xi_k}{2\pi\sigma_B(\boldsymbol{\xi})|\mathbf{x}-\boldsymbol{\xi}|^2}, \qquad k = 1,2,$$

and since ϕ is analytical when $\mathbf{x} \neq \boldsymbol{\xi}$ then the mixed derivatives coincide:

$$\begin{aligned}
\frac{\partial^2\phi(\mathbf{x},\boldsymbol{\xi})}{\partial x_1\partial\xi_1} &= \frac{1}{2\pi\sigma_B(\boldsymbol{\xi})^2}\frac{\partial\sigma_B(\boldsymbol{\xi})}{\partial\xi_1}\frac{x_1-\xi_1}{|\mathbf{x}-\boldsymbol{\xi}|^2} + \frac{(x_2-\xi_2)^2-(x_1-\xi_1)^2}{2\pi\sigma_B(\boldsymbol{\xi})|\mathbf{x}-\boldsymbol{\xi}|^4},\\
\frac{\partial^2\phi(\mathbf{x},\boldsymbol{\xi})}{\partial x_2\partial\xi_1} &= \frac{1}{2\pi\sigma_B(\boldsymbol{\xi})^2}\frac{\partial\sigma_B(\boldsymbol{\xi})}{\partial\xi_1}\frac{x_2-\xi_2}{|\mathbf{x}-\boldsymbol{\xi}|^2} - \frac{(x_1-\xi_1)\,(x_2-\xi_2)}{\pi\sigma_B(\boldsymbol{\xi})|\mathbf{x}-\boldsymbol{\xi}|^4},\\
\frac{\partial^2\phi(\mathbf{x},\boldsymbol{\xi})}{\partial x_1\partial\xi_2} &= \frac{1}{2\pi\sigma_B(\boldsymbol{\xi})^2}\frac{\partial\sigma_B(\boldsymbol{\xi})}{\partial\xi_2}\frac{x_1-\xi_1}{|\mathbf{x}-\boldsymbol{\xi}|^2} - \frac{(x_2-\xi_2)\,(x_1-\xi_1)}{\pi\sigma_B(\boldsymbol{\xi})|\mathbf{x}-\boldsymbol{\xi}|^4},\\
\frac{\partial^2\phi(\mathbf{x},\boldsymbol{\xi})}{\partial x_2\partial\xi_2} &= \frac{1}{2\pi\sigma_B(\boldsymbol{\xi})^2}\frac{\partial\sigma_B(\boldsymbol{\xi})}{\partial\xi_2}\frac{x_2-\xi_2}{|\mathbf{x}-\boldsymbol{\xi}|^2} + \frac{(x_1-\xi_1)^2-(x_2-\xi_2)^2}{2\pi\sigma_B(\boldsymbol{\xi})|\mathbf{x}-\boldsymbol{\xi}|^4}.
\end{aligned}$$

Denoting by superscript the partial derivative, we have two problems for the unknowns $\varphi_N^k = \partial\varphi_N/\partial\xi_k$, $k = 1,2$:

$$\begin{cases}
-\nabla_x \cdot \Big(\sigma_B(\mathbf{x})\nabla_1\varphi_N^k(\mathbf{x},\boldsymbol{\xi})\Big) = -\nabla_x \cdot \left(\Big(\sigma_B(\boldsymbol{\xi}) - \sigma_B(\mathbf{x})\Big)\boldsymbol{\Phi}^k(\mathbf{x},\boldsymbol{\xi})\right), & \mathbf{x} \text{ in } B,\\
\sigma_B(\mathbf{x})\,\nabla_1\varphi_N(\mathbf{x},\boldsymbol{\xi}) \cdot \boldsymbol{\nu} = -\sigma_B(\mathbf{x})\,\boldsymbol{\Phi}^k(\mathbf{x},\boldsymbol{\xi}) \cdot \boldsymbol{\nu} - \dfrac{1}{|\partial B|}, & \mathbf{x} \text{ on } \partial B,
\end{cases} \tag{2.13}$$

with

$$\boldsymbol{\Phi}^k(\mathbf{x},\boldsymbol{\xi}) = \left(\frac{\partial^2\phi(\mathbf{x},\boldsymbol{\xi})}{\partial x_1\partial\xi_k}, \frac{\partial^2\phi(\mathbf{x},\boldsymbol{\xi})}{\partial x_2\partial\xi_k}\right), \qquad \forall\,(\mathbf{x},\boldsymbol{\xi}) \in B \times B \,:\, \mathbf{x} \neq \boldsymbol{\xi}.$$

Remark 5. *All the second derivatives of ϕ are singular in $\mathbf{x} = \boldsymbol{\xi}$, and behave like $1/|\mathbf{x}-\boldsymbol{\xi}|^2$. Therefore, we can proceed as in Lemma 2 to show that the functional in* (2.13) *is bounded over $H^1(B)$, under the assumption $\alpha > 1$ in* (2.12).

3 Regularization techniques

In section 2.2 we showed the basis of the FM. Now we present some operative criteria to implement the range test. They are all based on the SVD decomposition of the operator $\widetilde{\Lambda}^{1/2}$. We focus mainly on the TR, although also a straightforward application of the PC in (2.8) can give good results.

Algorithm 1 The Factorization Method for EIT

Sample the probed region B with a set of points $R = \{\mathbf{y}_j\}_{j=1}^{P}$

for $\mathbf{y}$ in the set R **do**
  solve problem (1.5) to find its solution $N(\cdot, \mathbf{y})$,
  compute l_y^k from $N(\cdot, \mathbf{y})$ using (1.7),
  exploiting the information in l_y^k, decide if $\mathbf{y}$ belongs or not to D.
end for

The *SVD* decomposition of a real matrix $A \in \mathbb{R}^{m\times n}$ is

$$A = U\Sigma V^*,$$

where $U \in \mathbb{R}^{m\times m}$ and $V \in \mathbb{R}^{n\times n}$ are unitary matrices and $\Sigma \in \mathbb{R}^{m\times n}$ is a diagonal matrix containing the singular values σ_i, with $1 \le i \le \min(m,n)$. The columns of $U = (u_1|\dots|u_m)$ and $V = (v_1|\dots|v_n)$ are the singular vectors u_i, v_i which solve

$$A\,v_i = \sigma_i\,u_i, \qquad \text{and} \qquad A^* u_i = \sigma_i\,v_i.$$

3.1 Tikhonov regularization

In this section we need the adjoint of the operator $\widetilde{\Lambda}^{1/2}$, where $\widetilde{\Lambda}$ is defined in (1.4). To simplify the notation we rename it as $M = \widetilde{\Lambda}^{1/2}$. To check whether a given l_ξ^k belongs to $\mathrm{Range}\big(M\big)$ we have to solve the problem

$$Mg_\xi^k = l_\xi^k, \tag{3.1}$$

which demands for regularization. The key point is

$$\boldsymbol{\xi} \in D \quad \Longleftrightarrow \quad \Big(\|g_\xi^k\|_{L^2(\partial B)}\Big)^{-1} = 0.$$

The TR of (3.1) reads

$$\Big(\theta + M^*M\Big)g_\xi^k = M^* l_\xi^k. \tag{3.2}$$

In our case we choose the *Fourier basis* to discretize the operator M. It corresponds to take input currents in $\mathring{L}^2(\partial B)$ instead of $\mathring{H}^{-\frac{1}{2}}(\partial B)$. Accordingly the voltage will belong to $H^{\frac{3}{2}}(B)$, and thus our measured voltage will be in $H^1(\partial B)$ at least. Since we discretize l_ξ^k and g_ξ^k in (3.1) over the same orthogonal basis, then the discretization of M is a square matrix. This is a good choice in the case of the *Continuous Model*, but not for other models (*e.g.* the *Complete Electrode Model*).

In the following we denote by σ_i the singular values of M and by u_i and v_i the corresponding left and right singular vectors. Both the sets $\{u_i\}_{i=1}^{\infty}$ and $\{v_i\}_{i=1}^{\infty}$ are an orthonormal basis of $L^2(\partial B)$. Thus for any $\eta \in L^2(\partial B)$ we have:

$$M\eta = \sum_{i=1}^{\infty} \sigma_i(\eta, v_i)u_i, \qquad M^*\eta = \sum_{i=1}^{\infty} \sigma_i(\eta, u_i)v_i, \qquad (M^*M)\,\eta = \sum_{i=1}^{\infty} \sigma_i^2(\eta, v_i)v_i,$$

and applying this to problem (3.2) we get

$$M^* l_\xi^k = \sum_{i=1}^{\infty} \sigma_i (l_\xi^k, u_i) v_i, \qquad (M^* M) g_\xi^k = \sum_{i=1}^{\infty} \sigma_i^2 (g_\xi^k, v_i) v_i,$$

as well as the regularized solution

$$g_\xi^k = \sum_{i=1}^{\infty} \frac{\sigma_i}{\theta + \sigma_i^2} (l_\xi^k, u_i) v_i.$$

We choose the regularization parameter θ using the *Morozov principle*, *i.e.* imposing

$$\|M g_\xi^k - l_\xi^k\|_{L^2(\partial B)} = \delta, \tag{3.3}$$

with the parameter $\delta > 0$ to be related to the accuracy of the measurements. We pick

$$\delta = \gamma \sigma_1, \tag{3.4}$$

with σ_1 being the largest singular value of M and γ a given threshold. The term l_ξ^k depends on $\boldsymbol{\xi}$, so to ensure that (3.3) is uniformly satisfied we normalize l_ξ^k as $\hat{l}_\xi^k = l_\xi^k / \|l_\xi^k\|_{L^2(\partial B)}$. Since

$$\|M g_\xi^k - \hat{l}_\xi^k\|^2_{L^2(\partial B)} = \sum_{i=1}^{\infty} \Big(\frac{\sigma_i^2}{\theta + \sigma_i^2} - 1 \Big)^2 (\hat{l}_\xi^k, u_i)^2 = \sum_{i=1}^{\infty} \Big(\frac{\theta}{\theta + \sigma_i^2} \Big)^2 (\hat{l}_\xi^k, u_i)^2,$$

to impose (3.3) we solve the (truncated version of the) nonlinear equation

$$f(\theta) := \sum_{i=1}^{\infty} \frac{\theta^2}{(\theta + \sigma_i^2)^2} (\hat{l}_\xi^k, u_i)^2 - \delta^2 = 0. \tag{3.5}$$

The function $\theta \mapsto \|M g_\xi^k - l_\xi^k\|_{L^2(\partial B)}$ is monotonically increasing w.r.t. θ. If δ is sufficiently small then the solutions of (3.5) lie in a non-empty closed interval, see [10] for the proof.

3.2 Picard criterion

Another criterion to test the range condition is analyzed in [12]. It employs the function:

$$I_k(\boldsymbol{\xi}) = \frac{1}{\|l_\xi^k\|^2_{L^2(\partial B)}} \sum_{i=1}^{\infty} \frac{\Big| (l_\xi^k, u_i)_{L^2(\partial B)} \Big|^2}{|\sigma_i|^2}, \tag{3.6}$$

and it reads

$$\boldsymbol{\xi} \in D \quad \Longleftrightarrow \quad I_k(\boldsymbol{\xi}) < \infty.$$

The function (3.6) can be approximated by $\widetilde{I}_k(\boldsymbol{\xi}) \approx I_k(\boldsymbol{\xi})$ with

$$\widetilde{I}_k(\boldsymbol{\xi}) = \left(\sum_{i=1}^{m} \frac{\Big| (l_\xi^k, u_i)_{L^2(\partial B)} \Big|^2}{|\sigma_i|^2} \right) \Bigg/ \left(\sum_{i=1}^{m} \Big| (l_\xi^k, u_i)_{L^2(\partial B)} \Big|^2 \right), \tag{3.7}$$

retaining only the m largest singular values above the expected measurement error. Notice that the normalization of l_ξ^k is already embedded in (3.6). We refer to this criterion as the PC. It does not require to solve problem (3.1) to find its regularized solution.

3.3 Algebraic formulation

In the following we explain the steps to derive the algebraic formulation of problem (3.1) regularized with Tikhonov. Starting from (3.2) and using the SVD decomposition of $M = U\Sigma V^*$ we get $M^*\widehat{\Lambda} = V\Sigma U^* U\Sigma V^* = V\Sigma^2 V^*$, and $M^*\hat{l}_y^k = V\Sigma U^*\hat{l}_y^k$, so that from (3.2) it follows

$$\Big(\alpha I + V\Sigma^2 V^*\Big) g_y^k = \Big(\alpha VV^* + V\Sigma^2 V^*\Big) g_y^k = V\Big(\alpha I + \Sigma^2\Big) V^* g_y^k = V\Sigma U^*\hat{l}_y^k.$$

Defining the diagonal matrix R_α as

$$[R_\alpha]_{i,i} = \frac{\Sigma_{i,i}}{(\alpha + \Sigma_{i,i}^2)}$$

we get $V^* g_y^k = R_\alpha U^*\hat{l}_y^k$, or equivalently $g_y^k = VR_\alpha U^*\hat{l}_y^k$.

4 Numerical results

To show the results, we display the isolines of the indicator function

$$C(\boldsymbol{\xi}) = \left(\log\Big(v_1(\boldsymbol{\xi}) + v_2(\boldsymbol{\xi})\Big)\right)^{-1}, \tag{4.1}$$

where $v_k(\boldsymbol{\xi}) = \|g_\xi^k\|_{L^2(\partial B)}$ in the case of TR, or $v_k(\boldsymbol{\xi}) = \widetilde{I}_k(\boldsymbol{\xi})$ in the case of PC. A crucial point is the tuning of the scale and the choice of the isovalue that represents the inclusion. In practice, this requires additional information on the value of the diffusion coefficient in the inclusion. We plot the isolines of $C(\boldsymbol{\xi})$ in the range

$$\Big[C_{\min}^f, C_{\max}\Big] := \Big[f \cdot \min\{C(\boldsymbol{\xi}) \,:\, \boldsymbol{\xi} \in D\},\, \max\{C(\boldsymbol{\xi}) \,:\, \boldsymbol{\xi} \in D\}\Big],$$

using the parameter $0 < f < 1$. The step between the isolines is kept fixed, and this provides information also on the gradient of the indicator function. In all the numerical tests, the domain B is the unitary ball centered in $(0, 0)$. The sampling points consist of a 50×50 uniform grid over the square $[-1, 1] \times [-1, 1]$. In the FM we use only the points that fall at a distance larger than 0.05 from ∂B. In the test cases with small inclusions the resolution is increased to 100×100. The dashed purple line always marks the exact geometry of the inclusion(s).

As will be explained in the following, we need also to display the value of the indicator function (4.1). Thus we report also the plots with a color scale associated with the value of C.

4.1 The homogeneous case

The tests featuring a homogeneous background $\sigma_B = 1$ and $\sigma_D = 2$ are named with uppercase letters:

- *test case A:* a circular inclusion with radius 0.3 centered in $(0.3, 0.1)$;
- *test case B:* ten small circular inclusions with radius 0.025;
- *test case C:* two circular inclusions with radius 0.2 centered in $(-0.35, -0.35)$ and $(0.35, 0.35)$;
- *test case D:* an ellipsoidal inclusion centered in $(0.3, 0.1)$, with semiaxes 0.1 and 0.3.

Figure 3 displays the singular values of $\widetilde{\Lambda}^{1/2}$ in the aforementioned test cases. Then, Figures 4, 5, 6, 7 show the isolines of the indicator function (4.1) employing the TR or PC. The test case A is classic and does not show any significative differences between the TR and PC. If the value of the parameter γ is too low, then the isolines exhibit oscillations because the instability due to

the ill-posedness shows up. In the test case C the TR is less sensitive to the mutual disturbance between the two inclusions. Also in the test case D, the TR allows to recover the elongated shape, while the PC tends to reconstruct a circle. In the test case B both TR and PC can locate the outer inclusions, although the TR is more accurate and provides some information for the internal inclusions as well. See also a detailed zoom of the isolines near the inclusion in Figures 27, 28, 29, 30.

In the homogeneous case, it is possible to clearly detect the inclusion directly looking at the values of the optimal regularization parameter $\theta = \theta(\boldsymbol{\xi})$ which solves (3.5).

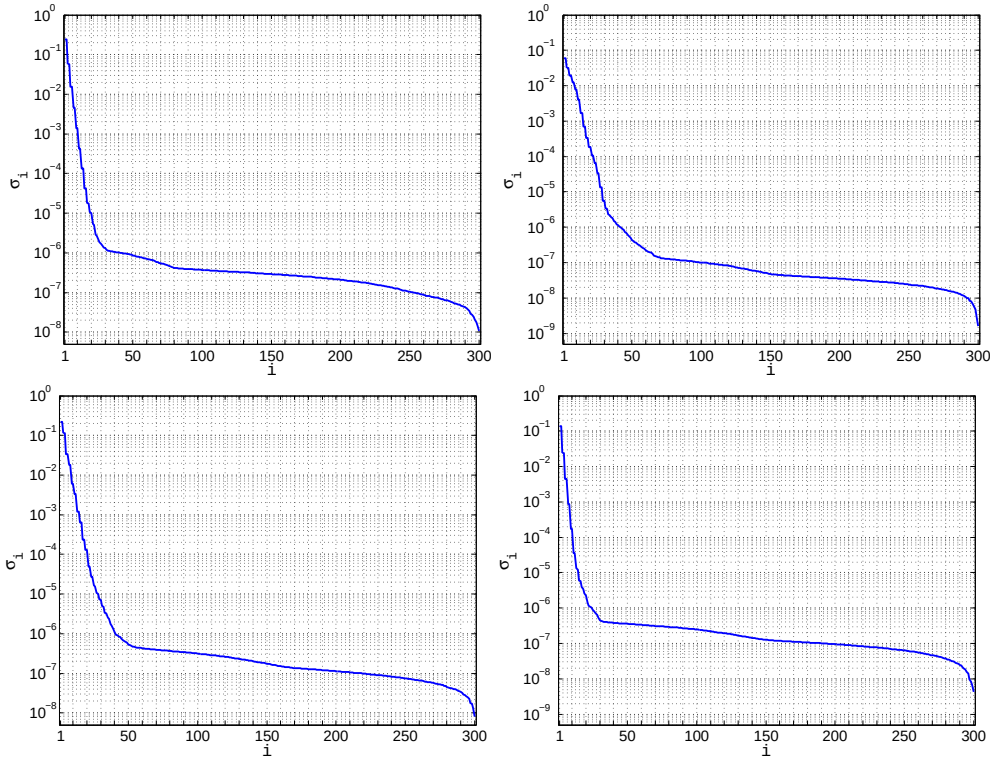

Fig. 3: Singular values σ_i of $\widetilde{\Lambda}^{1/2}$. Test case A (top-left). Test case B (top-right). Test case C (bottom-left). Test case D (bottom-right).

4.2 The inhomogeneous case

We proceed to test our numerical scheme (2.13) in some cases featuring an inhomogeneous background. Let us name with roman numbers the following tests:

- *test case I:* piecewise constant conductivity defined as in Fig. 9-Left. The radius of the concentric circle is 0.7. The inclusion is a circle with radius 0.1 centered in $(0.35, 0.35)$ and $\sigma_D = 10^{-3}$.
- *test case II:* piecewise constant conductivity defined as in Fig. 9-Right. The inclusion falls across the interface where the value of σ_B jumps by one order of magnitude. The radius of the concentric circles are 0.35 and 0.75. The inclusion is a circle with radius 0.1 centered in $(0, 0.33)$ and $\sigma_D = 10^{-3}$.
- *test case IIIa:* $\sigma_B(\boldsymbol{x}) = 1 + \beta\Big(\sin(5\,x_1) + \cos(5\,x_2)\Big)$, $\beta = 0.15$. The inclusion is a circle with radius 0.15 centered in $(-0.3, 0.3)$ and $\sigma_D = 2$.

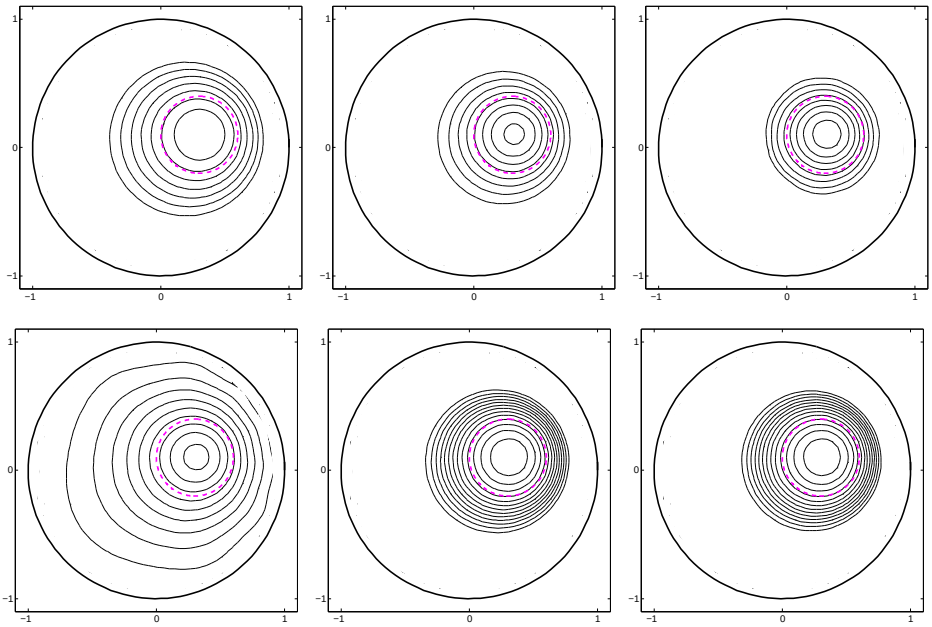

Fig. 4: Test case A. Isolines of $C(\boldsymbol{\xi})$ in $[C_{\min}^{0.5}, C_{\max}]$. Top: Tikhonov regularization: $\gamma = 5 \times 10^{-1}$ (left), $\gamma = 5 \times 10^{-2}$ (center), $\gamma = 5 \times 10^{-3}$ (right). Bottom: Picard criterion, $m = 5$ (left), $m = 25$ (center), $m = 50$ (right).

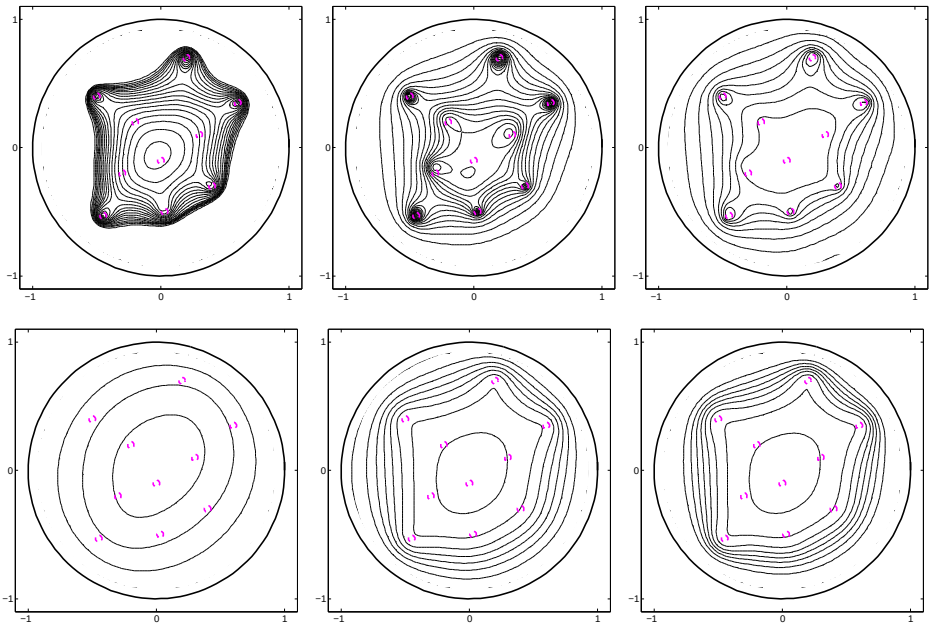

Fig. 5: Test case B. Isolines of $C(\boldsymbol{\xi})$ in $[C_{\min}^{0.5}, C_{\max}]$. Top: Tikhonov regularization, $\gamma = 10^{-2}$ (left), $\gamma = 10^{-3}$ (center), $\gamma = 10^{-4}$ (right). Bottom: Picard criterion, $m = 10$ (left), $m = 25$ (center), $m = 50$ (right).

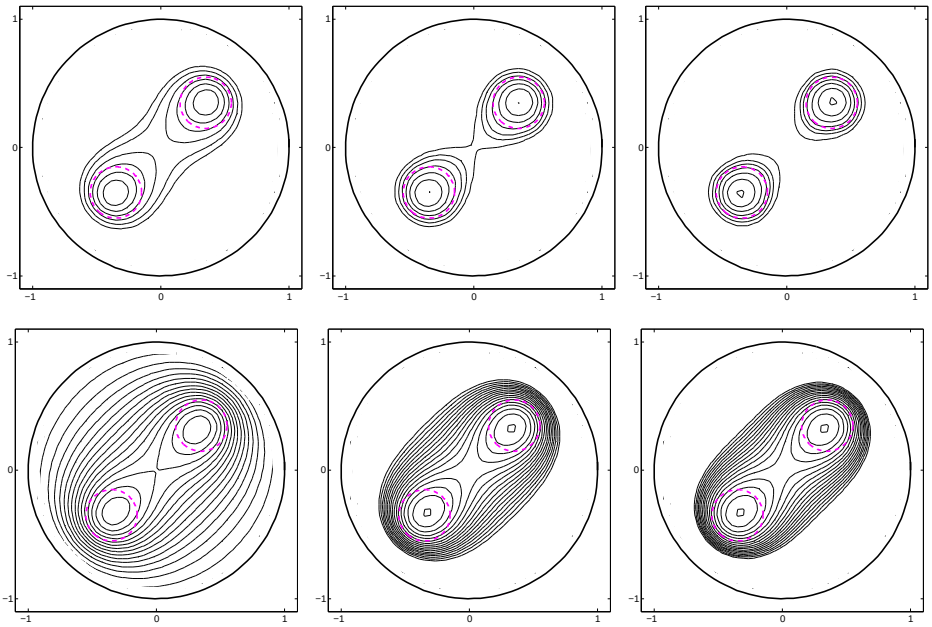

Fig. 6: Test case C. Isolines of $C(\boldsymbol{\xi})$ in $[C_{\min}^{0.6}, C_{\max}]$. Top: Tikhonov regularization with $\gamma = 5 \times 10^{-3}$ (left), $\gamma = 10^{-3}$ (center), $\gamma = 5 \times 10^{-4}$ (right). Bottom: Picard criterion. $m = 10$ (left), $m = 25$ (center), $m = 50$ (right).

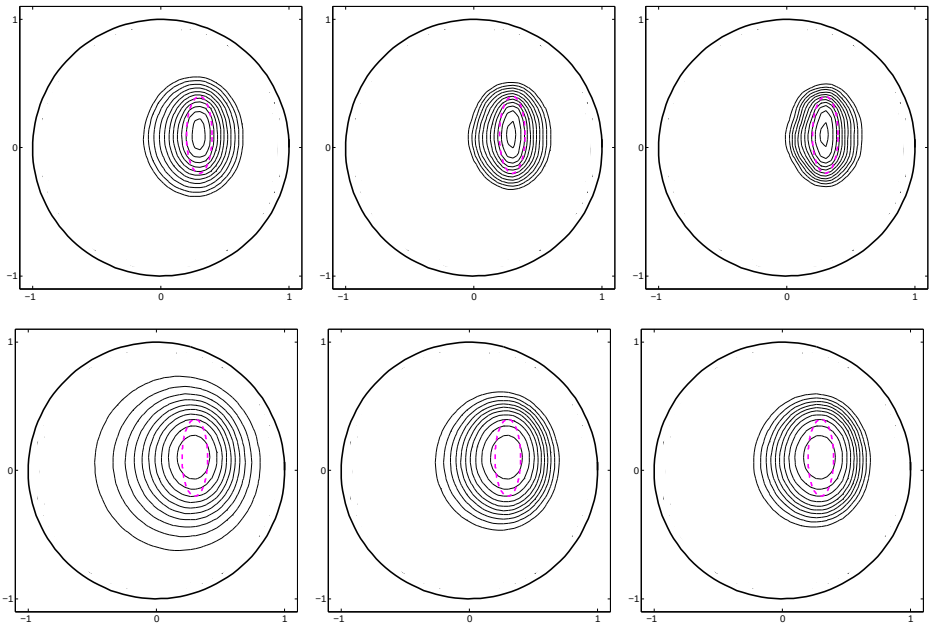

Fig. 7: Test case D. Isolines of $C(\boldsymbol{\xi})$ in $[C_{\min}^{0.5}, C_{\max}]$. Top: Tikhonov regularization with $\gamma = 5 \times 10^{-2}$ (left), $\gamma = 10^{-2}$ (center), $\gamma = 5 \times 10^{-3}$ (right). Bottom: Picard criterion. $m = 10$ (left), $m = 25$ (center), $m = 50$ (right).

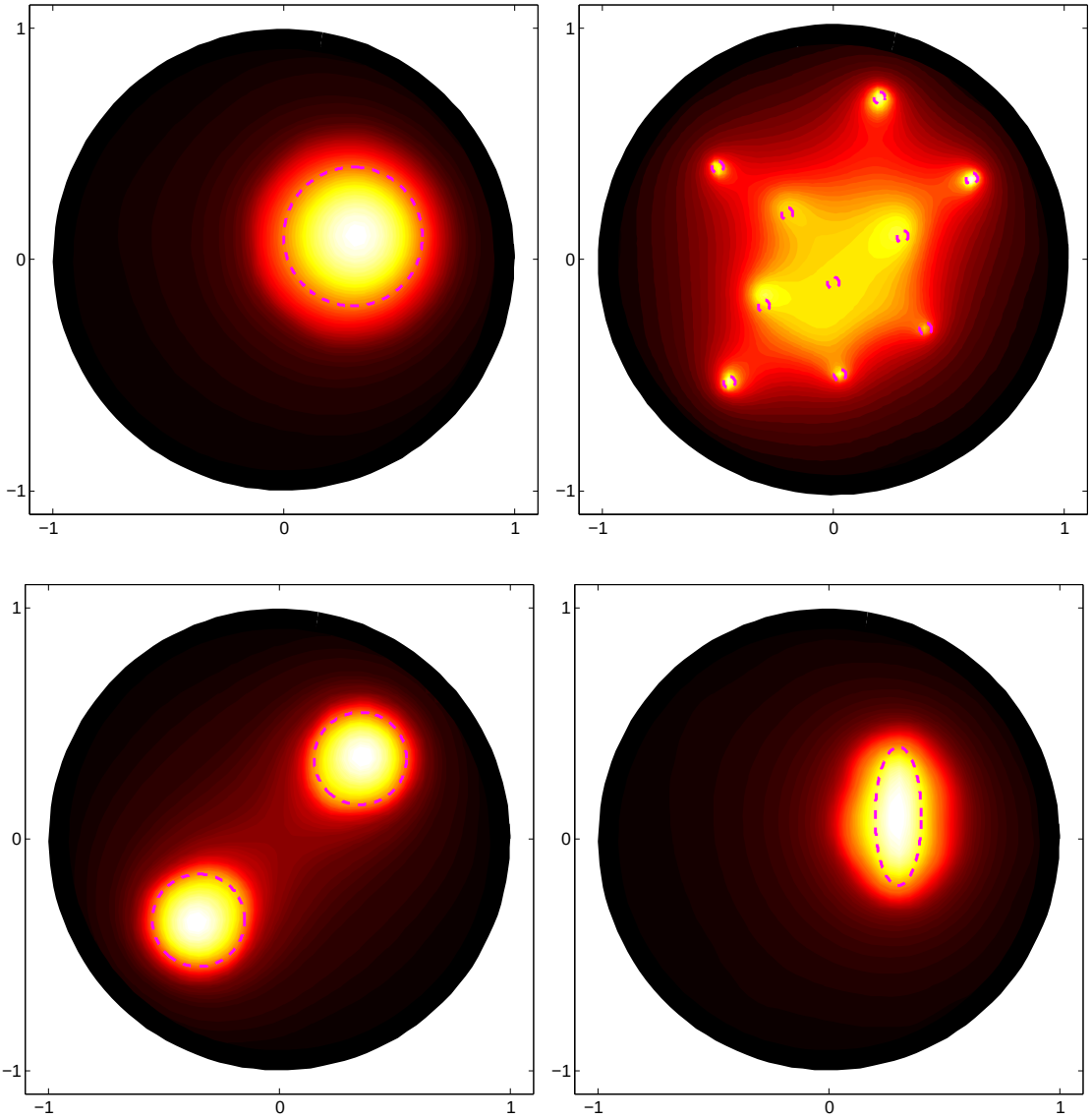

Fig. 8: Tikhonov regularization. Test case A, $\gamma = 5 \times 10^{-3}$ (top-left). Test case B, $\gamma = 10^{-3}$ (top-right). Test case C, $\gamma = 5 \times 10^{-4}$ (bottom-left). Test case D, $\gamma = 5 \times 10^{-3}$ (bottom-right).

- *test case IIIb:* same as the test case IIIa but with $\beta = 0.25$.
- *test case IVa:* ten small circular inclusions with radius (0.025), $\sigma_B(\boldsymbol{x}) = 1 + \beta\Big(\sin(5\,x_1) + \cos(5\,x_2)\Big)$, $\beta = 0.25$ and $\sigma_D = 2$.
- *test case IVb:* same as the test case IVa but with $\beta = 0.3$.
- *test case V:* one small circular inclusion with radius 0.025 centered in $(-0.3, 0.3)$, $\sigma_B(\boldsymbol{x}) = 5 \cdot (x_1 + x_2) + 11$ and $\sigma_D = 10^{-3}$.
- *test case VI:* $\sigma_B(\boldsymbol{x}) = 1 + (x_1^2 + x_2^2)$, $\sigma_D = 10^{-3}$. The inclusion is a circle with radius 0.15 centered in $(-0.3, 0.3)$.

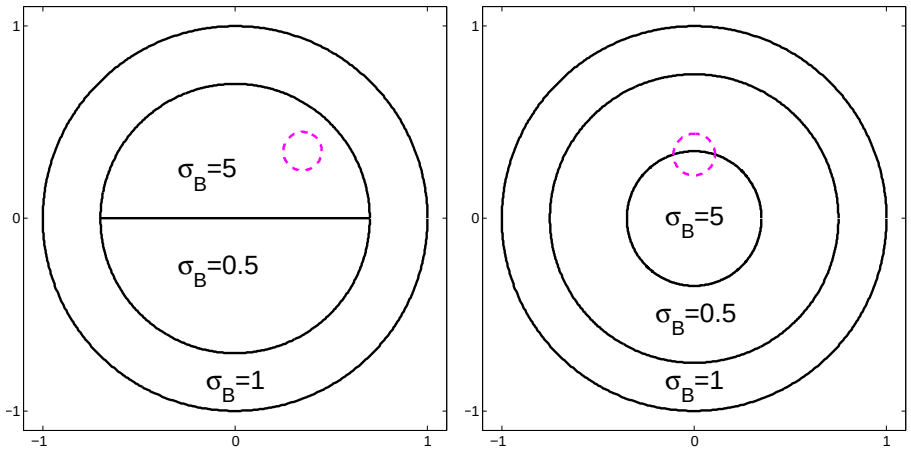

Fig. 9: Values of σ_B in the test case I (left) and in the test case II (right).

Again, we display the singular values of $\widetilde{\Lambda}^{1/2}$ for all the test cases in Figures 10 and 15. Despite the differences among the geometries and values of σ_B in the test cases, the singular values behave likewise. The most important difference is the order of magnitude of the largest singular values, since this affects the choice of the regularization parameters.

The numerical scheme (2.13) performs very well in the test cases I,II with a piecewise constant conductivity. In both cases σ_B jumps by one order of magnitude. In Figures 11,12 we reconstruct the inclusion using the TR and the PC. Figures 31,32,33-left show a zoom of the isolines near the inclusion.

In the test case IIIa the coefficient σ_B has a $\pm 30\%$ variation, and Figure 13 shows that both TR and PC are capable of accurately detecting the presence and location of the inclusion. See also in Figure 33-center a zoom near the inclusion.

The test case IIIb features the same geometries as the test case IIIa, but now σ_B has a $\pm 50\%$ variation. Still both TR and PC are able to detect the location of the inclusion (Figure 14), but the recovered shape begins to suffer a distortion, because of the strong nonlinearity in the coefficient. Analogously, in the test cases IVa and IVb the variations in σ_B are $\pm 50\%$ and $\pm 60\%$, respectively. As in the homogeneous case, the outer inclusions are well detected by both TR and PC, but only TR provides also some information in the internal region (Figures 16,17).

The test case V treats a linear coefficient σ_B that ranges between 4 and 18 approximately, while the test case VI treats a radial coefficient σ_B. As before (Figures 18,19), both TR and PC can accurately detect the presence and location of the inclusion.

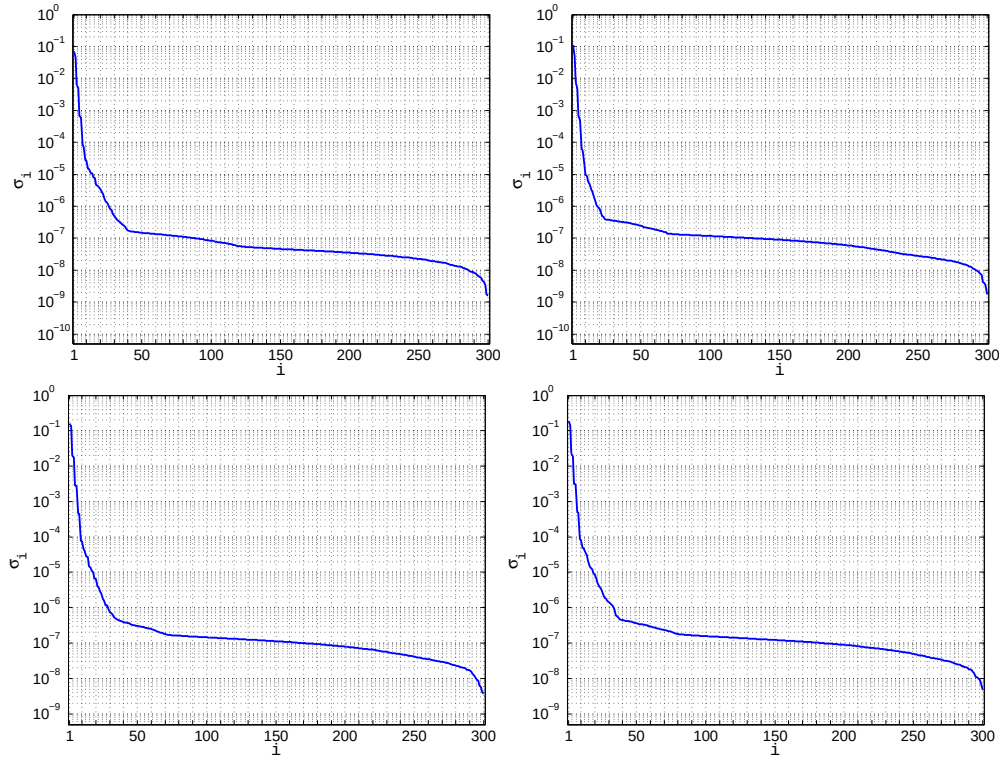

Fig. 10: Singular values σ_i of $\widetilde{\Lambda}^{1/2}$. Test case I (top-left). Test case II (top-right). Test case IIIa (bottom-left). Test case IIIb (bottom-right).

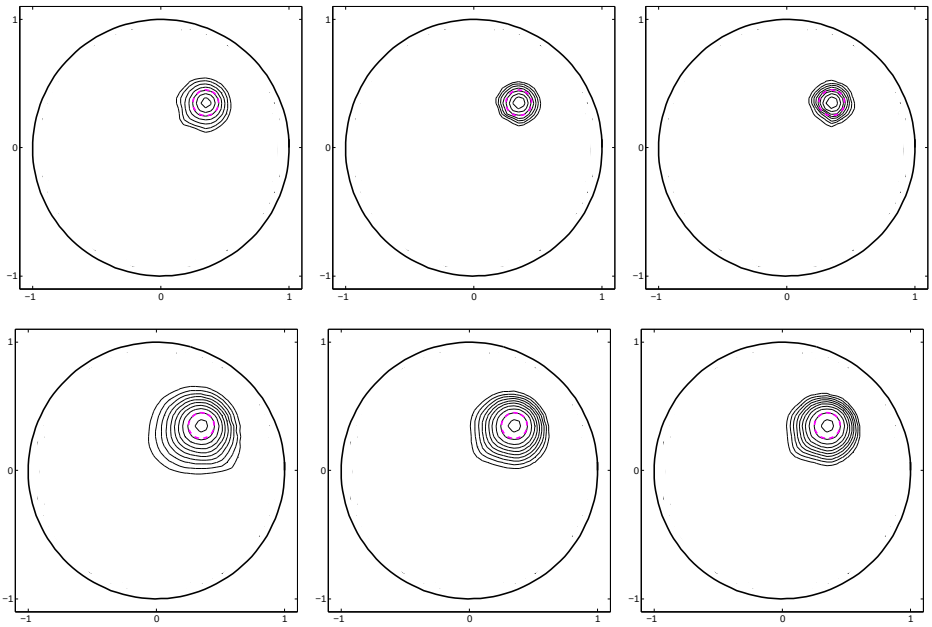

Fig. 11: Test case I. Isolines of $C(\boldsymbol{\xi})$ in $[C_{\min}^{0.6}, C_{\max}]$. Tikhonov regularization: $\gamma = 5 \times 10^{-2}$ (left), $\gamma = 10^{-2}$ (center), $\gamma = 5 \times 10^{-3}$ (right). Picard criterion, $m = 10$ (left), $m = 25$ (center), $m = 50$ (right).

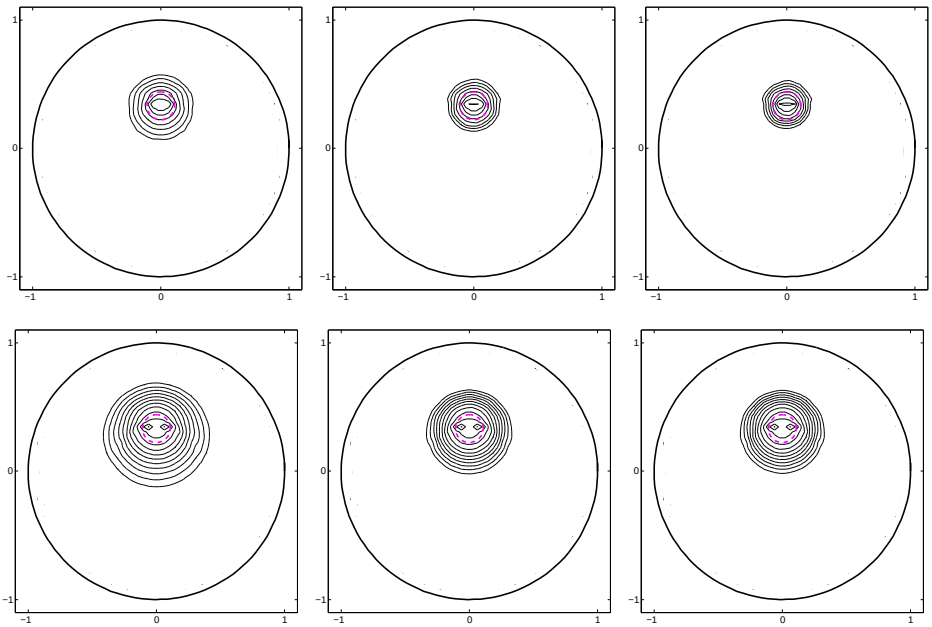

Fig. 12: Test case II. Isolines of $C(\boldsymbol{\xi})$ in $[C_{\min}^{0.6}, C_{\max}]$. Tikhonov regularization, $\gamma = 5\times10^{-2}$ (left), $\gamma = 10^{-2}$ (center), $\gamma = 5\times10^{-3}$ (right). Picard criterion, $m = 10$ (left), $m = 25$ (center), $m = 50$ (right).

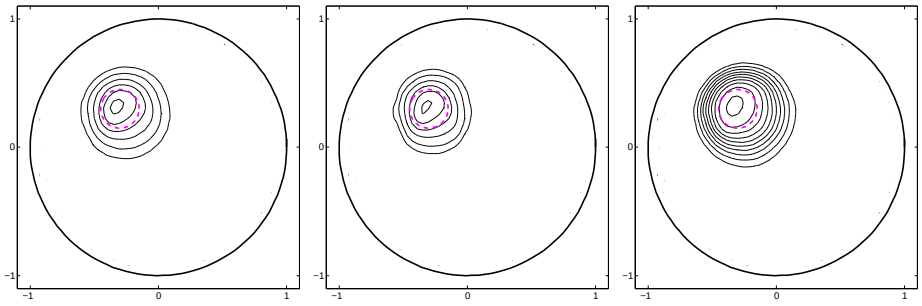

Fig. 13: Test case IIIa. Isolines of $C(\boldsymbol{\xi})$ in $[C_{\min}^{0.5}, C_{\max}]$. Left: Tikhonov regularization, $\gamma = 10^{-1}$. Center: Tikhonov regularization, $\gamma = 5\times10^{-2}$. Right: Picard criterion, $m = 25$.

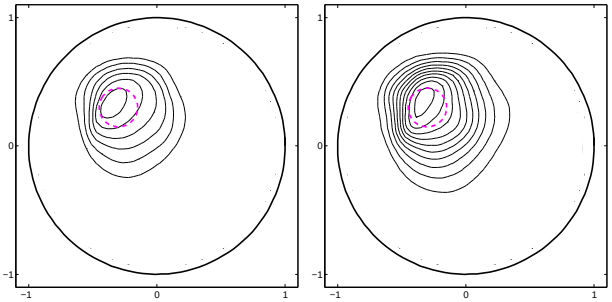

Fig. 14: Test case IIIb. Isolines of $C(\boldsymbol{\xi})$ in $[C_{\min}^{0.5}, C_{\max}]$. Left: Tikhonov regularization, $\gamma = 5\times10^{-1}$. Right: Picard criterion, $m = 10$.

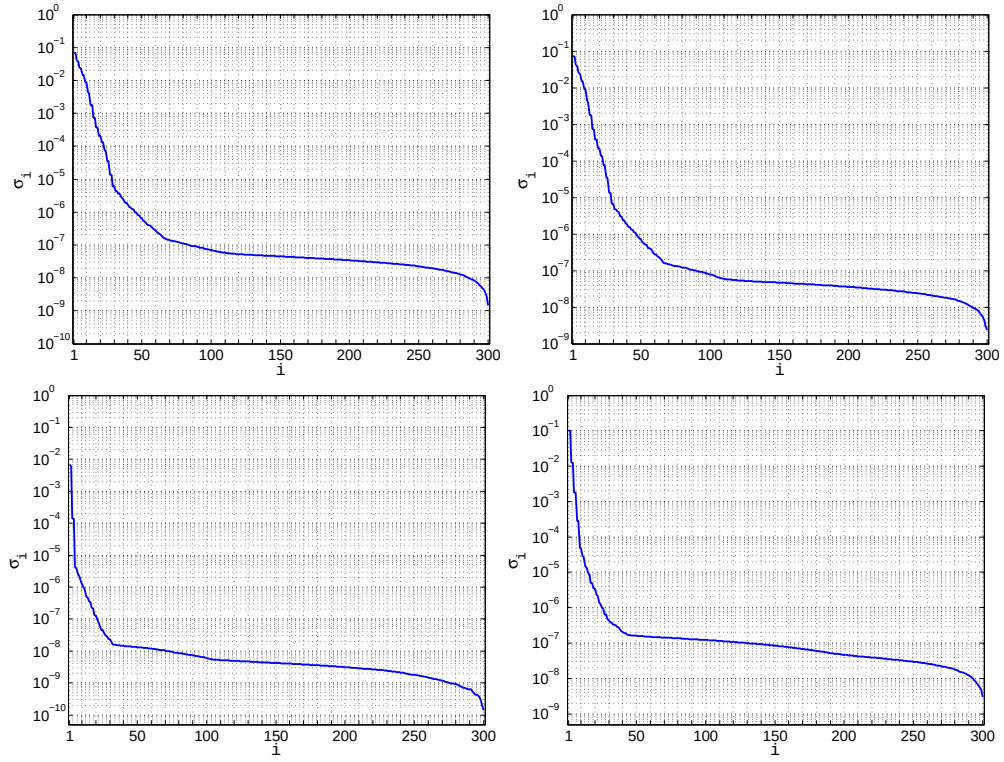

Fig. 15: Singular values σ_i of $\widetilde{\Lambda}^{1/2}$. Test case IVa (top-left). Test case IVb (top-right). Test case V (bottom-left). Test case VI (bottom-right).

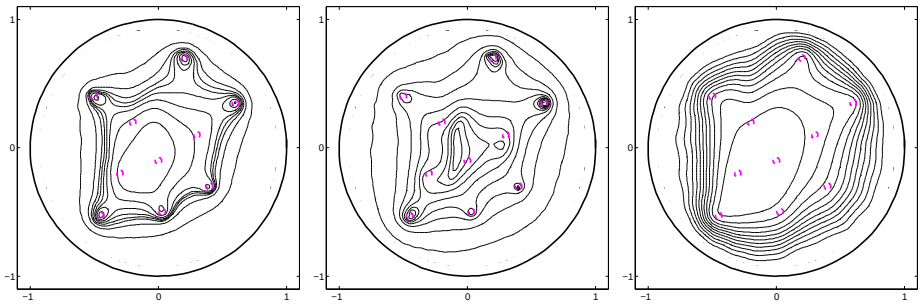

Fig. 16: Test case IVa. Isolines of $C(\boldsymbol{\xi})$. Left: Tikhonov regularization, $\gamma = 5 \times 10^{-3}$. Center: Tikhonov regularization, $\gamma = 10^{-3}$. Right: Picard criterion, $m = 25$.

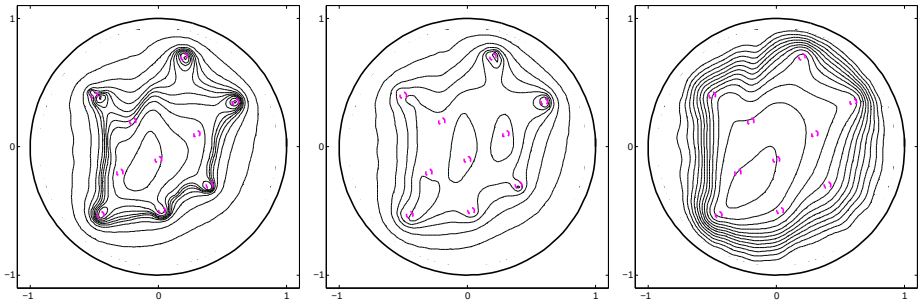

Fig. 17: Test case IVb. Isolines of $C(\boldsymbol{\xi})$. Left: Tikhonov regularization, $\gamma = 5 \times 10^{-3}$. Center: Tikhonov regularization, $\gamma = 10^{-3}$. Right: Picard criterion, $m = 25$.

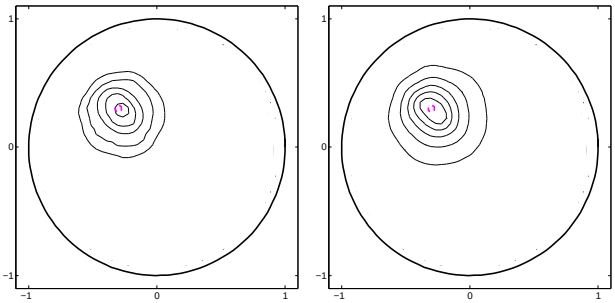

Fig. 18: Test case V. Isolines of $C(\boldsymbol{\xi})$ in $[C_{\min}^{0.7}, C_{\max}]$. Left: Tikhonov regularization, $\gamma = 5$. Right: Picard criterion, $m = 25$.

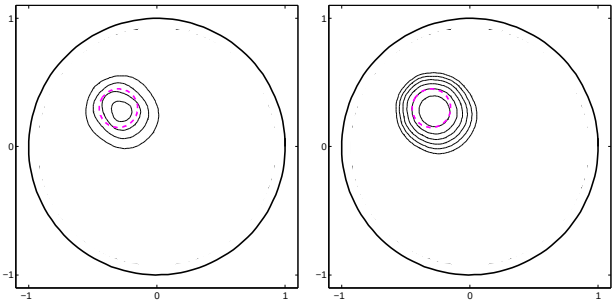

Fig. 19: Test case VI. Isolines of $C(\boldsymbol{\xi})$ in $[C_{\min}^{0.7}, C_{\max}]$. Left: Tikhonov regularization, $\gamma = 10^{-1}$. Right: Picard criterion, $m = 25$.

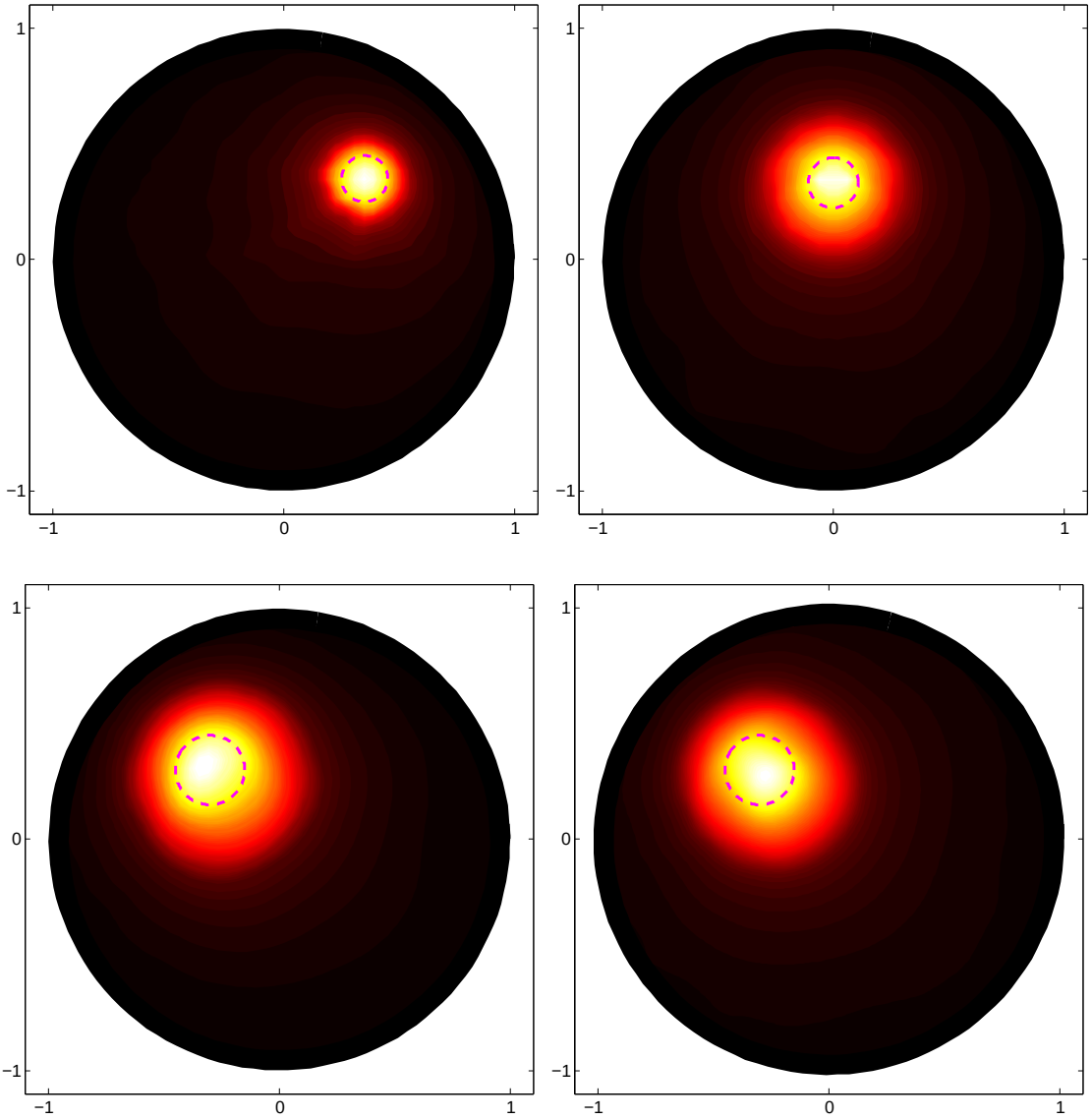

Fig. 20: Tikhonov regularization. Test case I, $\gamma = 10^{-2}$ (top-left). Test case II, $\gamma = 5 \times 10^{-2}$ (top-right). Test case IIIa, $\gamma = 10^{-1}$ (bottom-left). Test case VI, $\gamma = 10^{-2}$ (bottom-right).

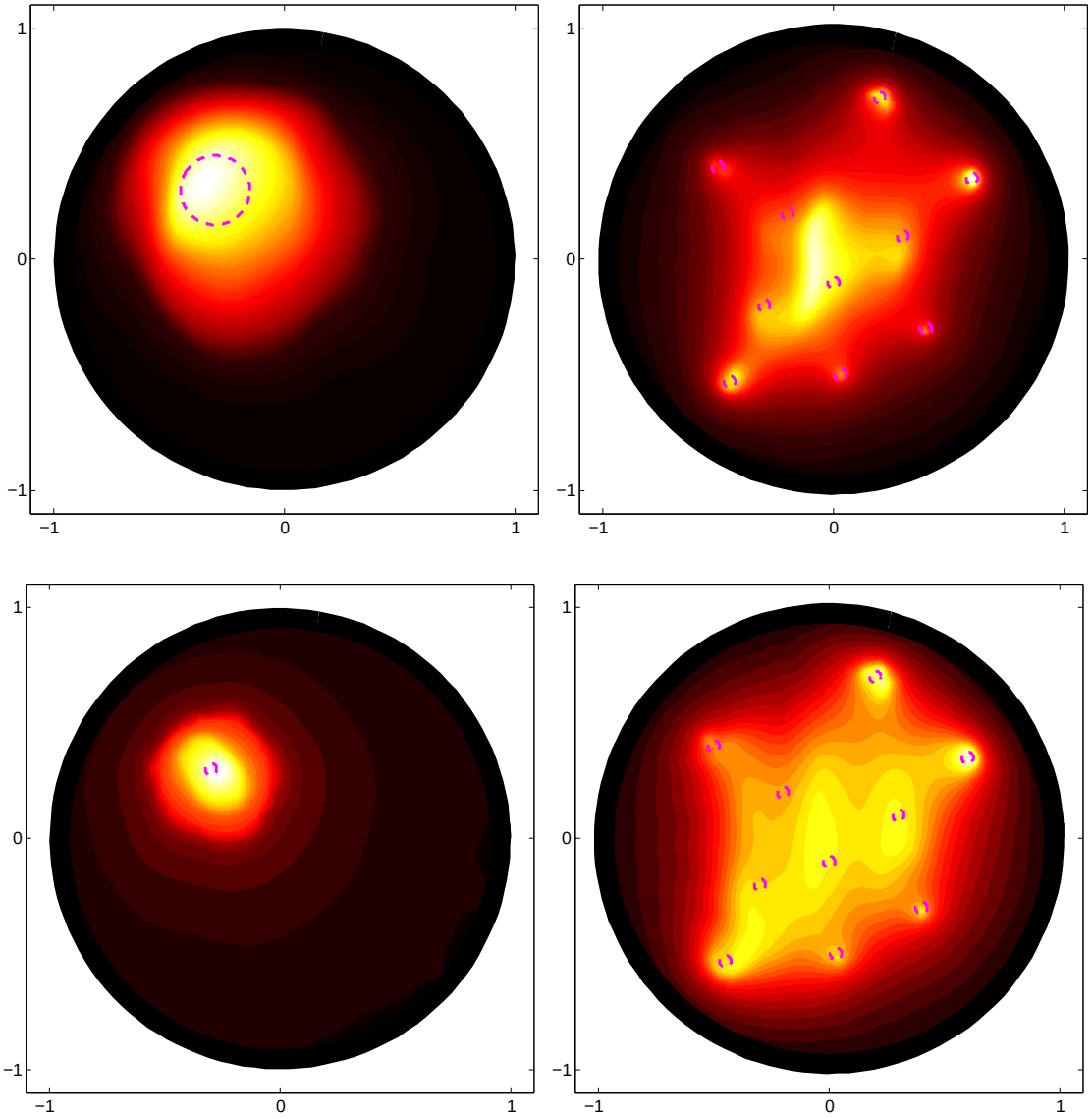

Fig. 21: Tikhonov regularization. Test case IIIb, $\gamma = 5 \times 10^{-1}$ (top-left). Test case IVa, $\gamma = 10^{-3}$ (top-right). Test case V, $\gamma = 5$ (bottom-left). Test case IVb, $\gamma = 10^{-3}$ (bottom-right).

4.3 Measures with noise

Now we investigate the sensitivity of our results to noisy perturbations. To this aim we perturb the operator M with the random matrix U, $U_{ij} \overset{\text{i.i.d.}}{\sim} \mathcal{U}([-1,1])$, scaled to the spectral norm of M:

$$M_\mu = M + \mu \|M\|_2 \frac{U}{\|U\|_2}. \tag{4.2}$$

The parameter μ represents the magnitude of the noisy perturbation, and accordingly we will tune γ in (3.4) or m in (3.7). In presence of noise the isolines obtained with the TR are identical to those obtained without noise, as long as a sufficient number of the largest singular values are not obfuscated. The effect of noise is an attenuation of the values in the indicator function (4.1). This holds also for a large amount of noise, up to 10%. Figures 22, 23, 24, 25, 26, show the results obtained for the test cases A,C,II,IIIa,IVa after adding 0.1% or 1% of noise. This correspond to pick $\mu = 10^{-3}$ or $\mu = 10^{-2}$, respectively, in (4.2). The indicator function (4.1) using the PC is attenuated a lot faster, preventing the recovery of the inclusion also for small amounts of noise. Therefore the TR should be preferred to the PC in case of noisy data.

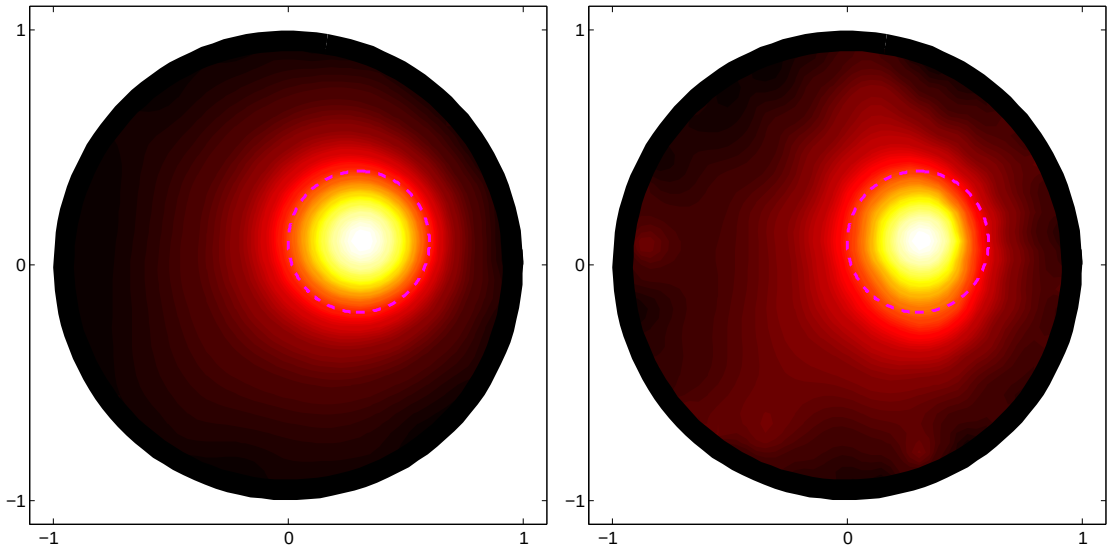

Fig. 22: Test case A. Tikhonov regularization, $\gamma = 5 \times 10^{-3}$. Left: 0.1% noise. Right: 1% noise.

5 Conclusions

We proposed a numerical scheme to solve the dipole-like Neumann problem featuring an inhomogeneous background coefficient. Then we incorporated this scheme in the Factorization Method applied to the Continuous Model for Electrical Impedance Tomography.

We have shown that the method accurately detects the presence and location of the inclusions, in cases where the background coefficient is piecewise constant with variations up to one order of magnitude, and in cases where the coefficient is nonlinearly dependent on the spatial coordinates. Two types of range test are compared, one based on the Tikhonov regularization and one based on the Picard criterion. The former performs more accurately, although in some cases also the latter yields a precise reconstruction. The method also proved to be robust within a reasonable range of noisy perturbations.

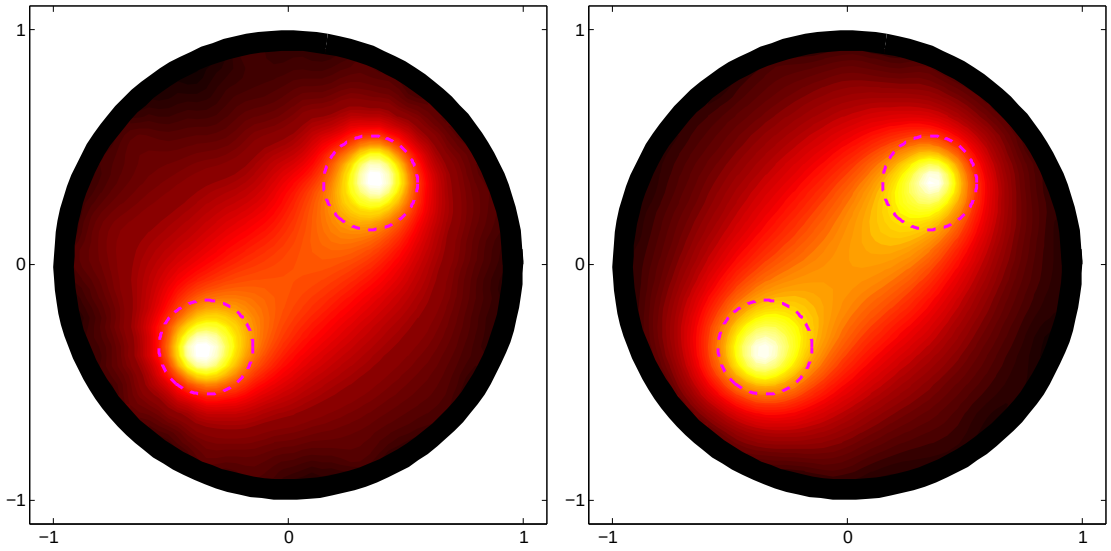

Fig. 23: Test case C. Tikhonov regularization, $\gamma = 5 \times 10^{-4}$. Left: 0.1% noise. Right: 1% noise.

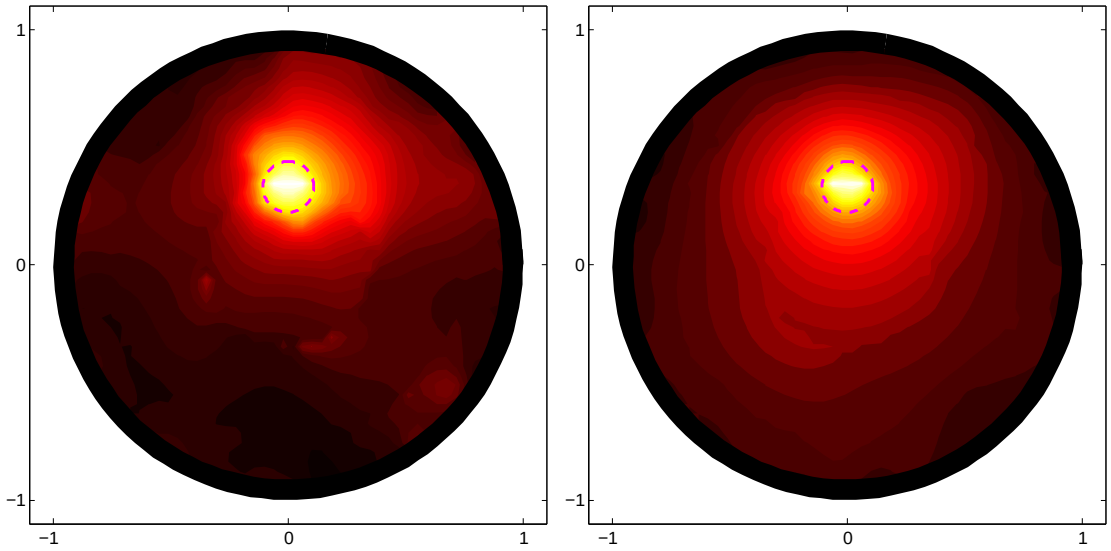

Fig. 24: Test case II. Tikhonov regularization, $\gamma = 5 \times 10^{-2}$. Left: 0.1% noise. Right: 1% noise.

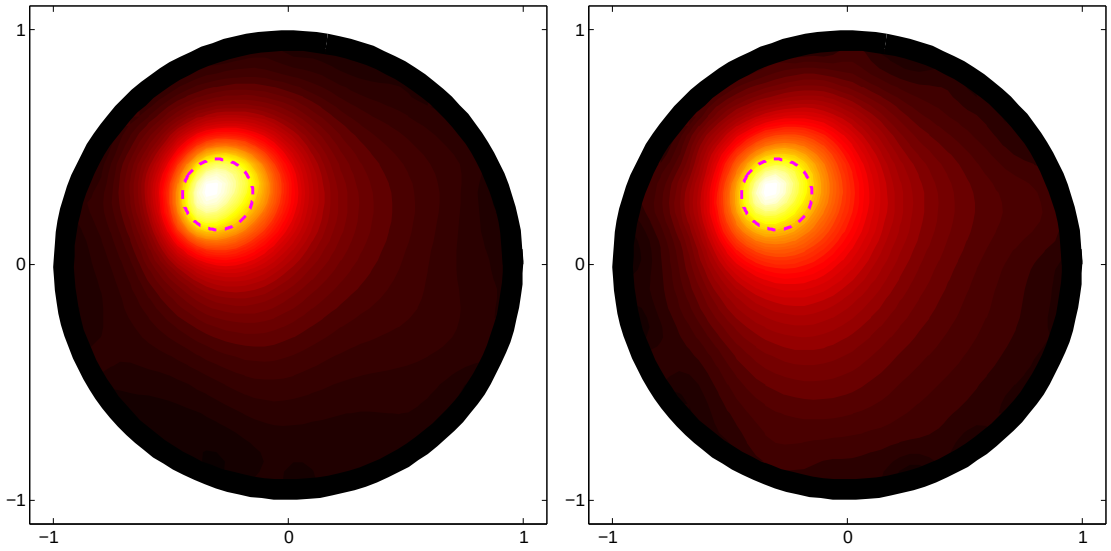

Fig. 25: Test case IIIa. Tikhonov regularization, $\gamma = 10^{-1}$. Left: 0.1% noise. Right: 1% noise.

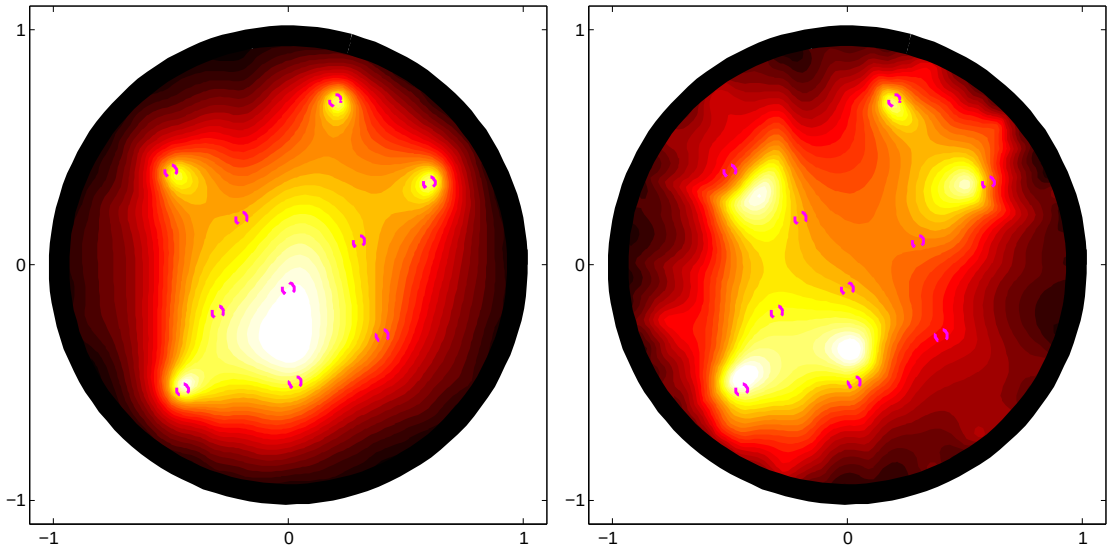

Fig. 26: Test case IVa. Tikhonov regularization, $\gamma = 10^{-3}$. Left: 0.1% noise. Right: 1% noise.

A Exact geometries

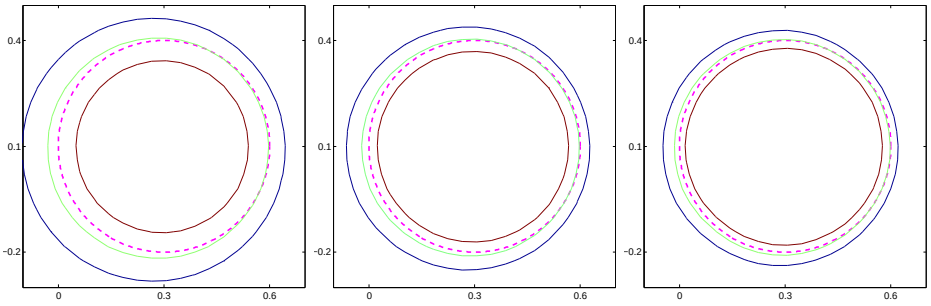

Fig. 27: Test case A. Exact geometry (dashed purple line), isolines $C^{0.9}_{\min}$ (blue), $C^{1}_{\min}$ (green), $C^{1.1}_{\min}$ (brown). Tikhonov regularization: $\gamma = 5 \times 10^{-1}$ (left), $\gamma = 5 \times 10^{-2}$ (center), $\gamma = 5 \times 10^{-3}$ (right).

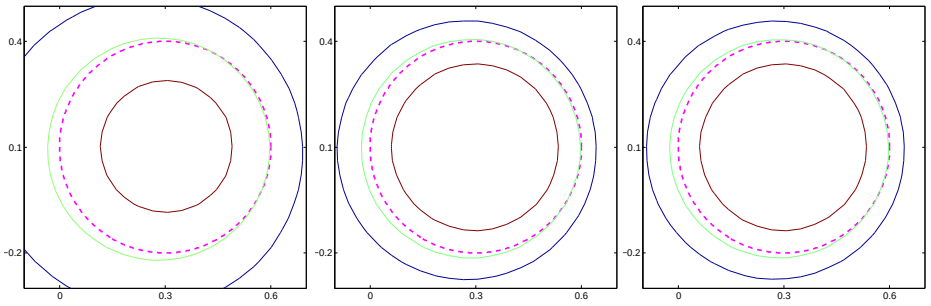

Fig. 28: Test case A. Exact geometry (dashed purple line), isolines $C^{0.9}_{\min}$ (blue), $C^{1}_{\min}$ (green), $C^{1.1}_{\min}$ (brown). Picard criterion, $m = 5$ (left), $m = 25$ (center), $m = 50$ (right).

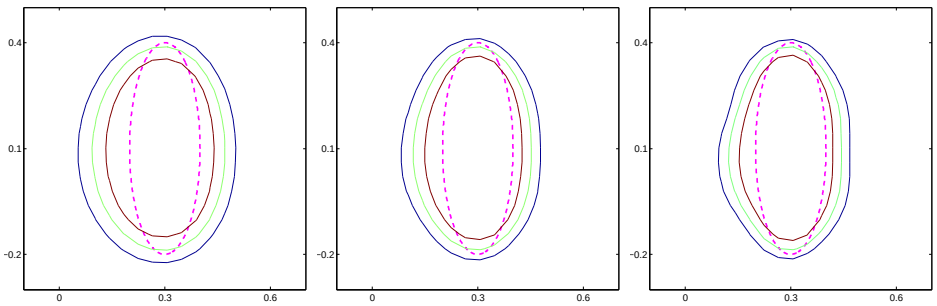

Fig. 29: Test case D. Exact geometry (dashed purple line), isolines $C^{0.9}_{\min}$ (blue), $C^{1}_{\min}$ (green), $C^{1.1}_{\min}$ (brown). Tikhonov regularization with $\gamma = 5 \times 10^{-2}$ (left), $\gamma = 10^{-2}$ (center), $\gamma = 5 \times 10^{-3}$ (left).

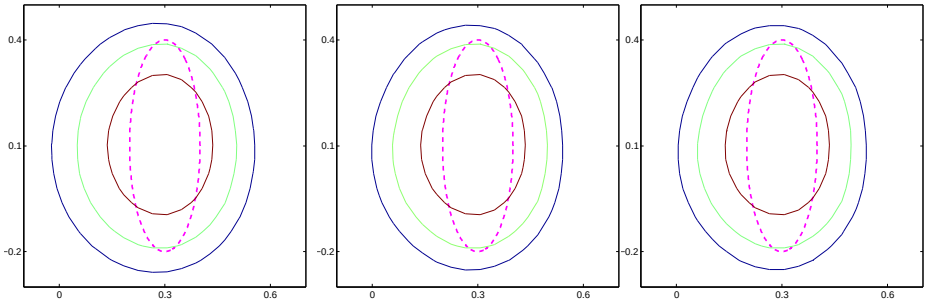

Fig. 30: Test case D. Exact geometry (dashed purple line), isolines $C^{0.9}_{\min}$ (blue), $C^{1}_{\min}$ (green), $C^{1.1}_{\min}$ (brown). Picard criterion, $m = 10$ (left), $m = 30$ (center), $m = 50$ (right).

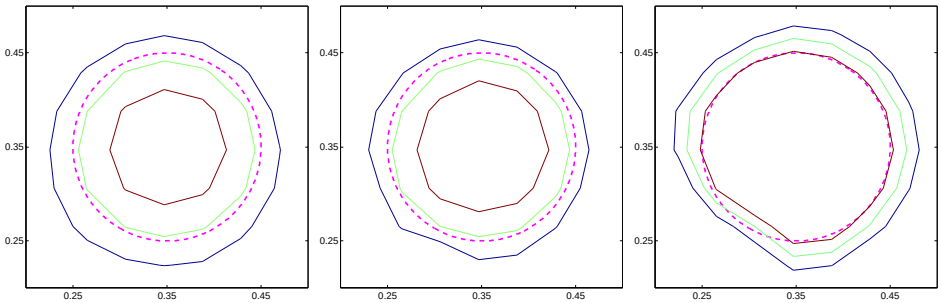

Fig. 31: Test case I. Exact geometry (dashed purple line), isolines $C^{0.9}_{\min}$ (blue), $C^{1}_{\min}$ (green), $C^{1.1}_{\min}$ (brown). Tikhonov regularization: $\gamma = 5 \times 10^{-2}$ (left), $\gamma = 10^{-3}$ (center), $\gamma = 5 \times 10^{-3}$ (right).

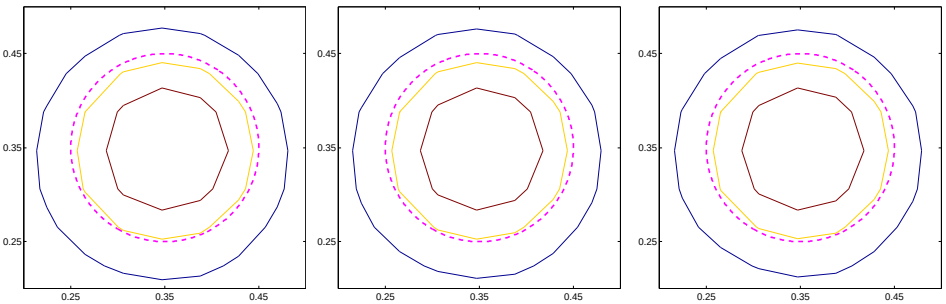

Fig. 32: Test case I. Exact geometry (dashed purple line), isolines $C^{0.95}_{\min}$ (blue), $C^{1}_{\min}$ (orange), $C^{1.025}_{\min}$ (brown). Picard criterion, $m = 10$ (left), $m = 25$ (center), $m = 50$ (right).

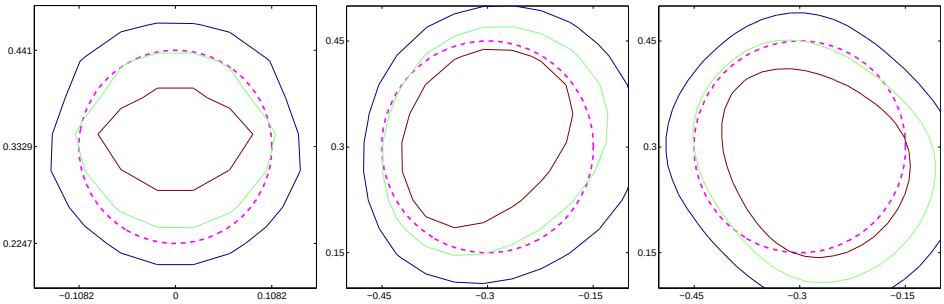

Fig. 33: Exact geometry (dashed purple line), isolines $C^{0.9}_{\min}$ (blue), $C^{1}_{\min}$ (green), $C^{1.1}_{\min}$ (brown). Test case II, Tikhonov regularization, $\gamma = 5 \times 10^{-2}$. Test case IIIa, Tikhonov regularization, $\gamma = 10^{-1}$. Test case VI, Tikhonov regularization, $\gamma = 10^{-1}$.

B Well-posedness and regularity issue

We recall some regularity results for elliptic problems in the form

$$\begin{cases} -\nabla \cdot \Big(\sigma(\mathbf{x})\nabla u(\mathbf{x})\Big) = f(\mathbf{x}), & \mathbf{x} \text{ in } \Omega, \\ \sigma(\mathbf{x})\nabla u(\mathbf{x}) \cdot \boldsymbol{\nu} = h(\mathbf{x}), & \mathbf{x} \text{ on } \partial\Omega, \end{cases} \tag{B.1}$$

under the assumptions:

- Ω bounded subset of $\mathbb{R}^2$,
- $\sigma_{\min}|\boldsymbol{\zeta}|^2 \leq \sigma(\mathbf{x})\,\boldsymbol{\zeta}\cdot\boldsymbol{\zeta} \leq \sigma_{\max}|\boldsymbol{\zeta}|^2, \quad \forall\,\boldsymbol{\zeta}\in\mathbb{R}^2, \quad$ almost everywhere in Ω,
- $f \in L^2(\Omega)$.

Problem (1.2) is an example of (B.1), while problem (1.5) reduces to (B.1) if the singularity in $\boldsymbol{\xi}$ is removed. The proofs of the following results can be found in [11].

Theorem 10. *Given a bounded Lipschitz domain Ω, if $f \in L^2(\Omega)$ and $g \in L^2(\partial\Omega)$ then one of the following alternatives hold:*

- *problem* (B.1) *has a unique solution $u \in H^1(\Omega)$ and*

$$\|u\|_{H^1(\Omega)} \leq C(\sigma_{min}, \sigma_{max})\Big(\|f\|_{L^2(\Omega)} + \|h\|_{L^2(\partial\Omega)}\Big),$$

- *the homogeneous problem* (B.1) *(with $f \equiv 0$ and $h \equiv 0$) and its adjoint homogeneous problem have each the same finite number of linearly independent solutions.*

Moreover, problem (B.1) *has a solution* if and only if

$$\int_\Omega f w\, d\mathbf{x} + \int_{\partial\Omega} h w\, d\sigma = 0, \tag{B.2}$$

for every solution w of the adjoint homogeneous problem associated with (B.1).

One can show that the solutions of the adjoint homogeneous problem associated with (B.1) are the constant functions. Thus from (B.2) we recover the usual compatibility condition.

Theorem 11 (H^2 interior regularity of the solution of problem (B.1))**.** *If the components of the coefficient $\sigma(\mathbf{x})$ are Lipschitz in Ω, then the solution $u \in H^2_{loc}(\Omega)$. Moreover, if $\Omega' \subset\subset \Omega$ then*

$$\|u\|_{H^2(\Omega')} \leq C(\sigma_{min}, \sigma_{max}, dist(\partial\Omega, \Omega'), K)\left(\|f\|_{L^2(\Omega)} + \|u\|_{L^2(\Omega)}\right),$$

where K is the Lipschitz constant of $\sigma(\cdot)$.

Theorem 11 shows that u is a strong solution. Increasing the regularity of the data the solution also increases its regularity.

Theorem 12 (Global regularity of the solution of problem (B.1))**.** *Let Ω be a bounded C^2–domain in $\mathbb{R}^2$. If the components of the coefficient $\sigma(\mathbf{x})$ are Lipschitz in Ω and $f(\mathbf{x}) \in L^2(\Omega)$, then $u \in H^2(\Omega)$ and*

$$\|u\|_{H^2(\Omega)} \leq C\left(\|f\|_{L^2(\Omega)} + \|u\|_{L^2(\Omega)} + \|h\|_{H^{1/2}(\partial\Omega)}\right),$$

where K is the Lipschitz constant of $\sigma(\cdot)$.

Theorem 13 (Higher global regularity of the solution to problem (B.1))**.** *Given $m \geq 1$, let Ω be a bounded C^{m+2}–domain in $\mathbb{R}^2$. If*

$$\sigma(\mathbf{x})_{ij} \in C^{m+1}(\overline{\Omega}), \qquad f(\mathbf{x}) \in H^m(\Omega) \qquad \text{and} \qquad h \in C^{m+1/2}(\partial\Omega),$$

then $u \in H^{m+2}(\Omega)$ and

$$\|u\|_{H^{m+2}(\Omega)} \leq C\left(\|f\|_{H^m(\Omega)} + \|u\|_{L^2(\Omega)} + \|h\|_{H^{m+1/2}(\partial\Omega)} \right).$$

From Theorem 13 we see that if Ω is a C^∞–domain, $\sigma(\mathbf{x})_{ij} \in C^\infty(\overline{\Omega})$, $f(\mathbf{x}) \in C^\infty(\Omega)$ and $h \in C^\infty(\partial\Omega)$ then $u \in C^\infty(\overline{\Omega})$.

References

[1] Giovanni Alessandrini. Stable determination of conductivity by boundary measurements. *Appl. Anal.*, 27(1-3):153–172, 1988.

[2] Habib Ammari and Hyeonbae Kang. *Polarization and moment tensors*, volume 162 of *Applied Mathematical Sciences*. Springer, New York, 2007.

[3] Kari Astala and Lassi Päivärinta. Calderón's inverse conductivity problem in the plane. *Ann. of Math. (2)*, 163(1):265–299, 2006.

[4] Mustapha Azzouz, Martin Hanke, Chantal Oesterlein, and Karl Schilcher. The factorization method for electrical impedance tomography data from a new planar device. *International Journal of Biomedical Imaging*, 2007.

[5] Russell M. Brown and Rodolfo H. Torres. Uniqueness in the inverse conductivity problem for conductivities with 3/2 derivatives in L^p, $p > 2n$. *J. Fourier Anal. Appl.*, 9(6):563–574, 2003.

[6] Martin Brühl. Explicit characterization of inclusions in electrical impedance tomography. *SIAM J. Math. Anal.*, 32(6):1327–1341 (electronic), 2001.

[7] Martin Brühl, Martin Hanke, and Michael S. Vogelius. A direct impedance tomography algorithm for locating small inhomogeneities. *Numer. Math.*, 93(4):635–654, 2003.

[8] Alberto-P. Calderón. On an inverse boundary value problem. In *Seminar on Numerical Analysis and its Applications to Continuum Physics (Rio de Janeiro, 1980)*, pages 65–73. Soc. Brasil. Mat., Rio de Janeiro, 1980.

[9] D. J. Cedio-Fengya, S. Moskow, and M. S. Vogelius. Identification of conductivity imperfections of small diameter by boundary measurements. Continuous dependence and computational reconstruction. *Inverse Problems*, 14(3):553–595, 1998.

[10] Heinz W. Engl, Martin Hanke, and Andreas Neubauer. *Regularization of inverse problems*, volume 375 of *Mathematics and its Applications*. Kluwer Academic Publishers Group, 1996.

[11] Lawrence C. Evans. *Partial Differential Equations*. American Mathematical Society, 1997.

[12] Bastian Gebauer and Nuutti Hyvönen. Factorization method and irregular inclusions in electrical impedance tomography. *Inverse Problems*, 23(5):2159–2170, 2007.

[13] Martin Hanke and Birgit Schappel. The factorization method for electrical impedance tomography in the half-space. *SIAM J. Appl. Math.*, 68(4):907–924, 2008.

[14] Andreas Kirsch and Natalia Grinberg. *The factorization method for inverse problems*. Oxford University Press, 2008.

[15] Armin Lechleiter, Nuutti Hyvönen, and Harri Hakula. The factorization method applied to the complete electrode model of impedance tomography. *SIAM J. Appl. Math.*, 68(4):1097–1121, 2008.

[16] John M. Lee and Gunther Uhlmann. Determining anisotropic real-analytic conductivities by boundary measurements. *Comm. Pure Appl. Math.*, 42(8):1097–1112, 1989.

[17] O. Scherzer, editor. *Handbook of Mathematical methods in Imaging*. Springer, 2010.

[18] Y. Zou and Z. Guo. A review of electrical impedance techniques for breast cancer detection. *Medical Engineering and Physics*, 25(2):79 – 90, 2003.

Centre de recherche INRIA Saclay – Île-de-France
Parc Orsay Université - ZAC des Vignes
4, rue Jacques Monod - 91893 Orsay Cedex (France)

Centre de recherche INRIA Bordeaux – Sud Ouest : Domaine Universitaire - 351, cours de la Libération - 33405 Talence Cedex
Centre de recherche INRIA Grenoble – Rhône-Alpes : 655, avenue de l'Europe - 38334 Montbonnot Saint-Ismier
Centre de recherche INRIA Lille – Nord Europe : Parc Scientifique de la Haute Borne - 40, avenue Halley - 59650 Villeneuve d'Ascq
Centre de recherche INRIA Nancy – Grand Est : LORIA, Technopôle de Nancy-Brabois - Campus scientifique
615, rue du Jardin Botanique - BP 101 - 54602 Villers-lès-Nancy Cedex
Centre de recherche INRIA Paris – Rocquencourt : Domaine de Voluceau - Rocquencourt - BP 105 - 78153 Le Chesnay Cedex
Centre de recherche INRIA Rennes – Bretagne Atlantique : IRISA, Campus universitaire de Beaulieu - 35042 Rennes Cedex
Centre de recherche INRIA Sophia Antipolis – Méditerranée : 2004, route des Lucioles - BP 93 - 06902 Sophia Antipolis Cedex

Éditeur
INRIA - Domaine de Voluceau - Rocquencourt, BP 105 - 78153 Le Chesnay Cedex (France)
http://www.inria.fr
ISSN 0249-6399